Univerzita Karlova v Praze
Matematicko-fyzikální fakulta

DIPLOMOVÁ PRÁCE

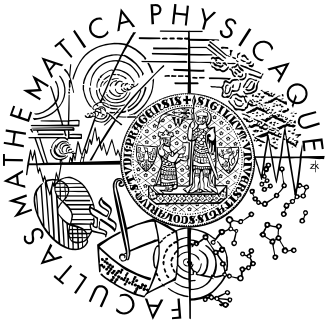

Martin Rusňák

Strukturní nespojitost v hexagonálních látkách typu RTX

Katedra fyziky kondenzovaných látek

Vedoucí diplomové práce: RNDr. Jiří Prchal, Ph.D.

Studijní program: Fyzika, Fyzika kondenzovaných soustav a materiálů

2010

Charles University in Prague
Faculty of Mathematics and Physics

DIPLOMA THESIS

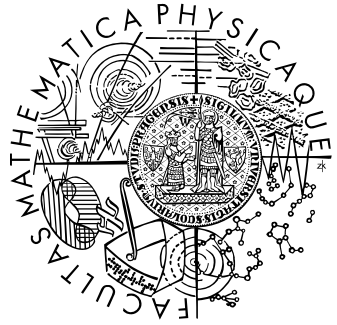

Martin Rusňák

Structure discontinuity in the RTX hexagonal materials

Department of Condensed Matter Physics

Supervisor: RNDr. Jiří Prchal, Ph.D.

Study program: Physics, Physics of Condensed Matter and Materials

2010

I would like to thank to supervisor of my work RNDr. Jiří Prchal, Ph.D. for his help on the whole thesis. If it were measurements, their analysis, explanation of the theory behind the studied subject, positive motivation or process of creation of the thesis itself RNDr. Jiří Prchal, Ph.D. was always there willing to help me.

My thanks belong to Mgr. Jiří Pospíšil, for his help with preparation, analyzation orientation of the samples, Dr. Hideaki Kitazawa for his assistance with the low-temperature X-ray diffraction experiment, doc. RNDr. Stanislavov Daniš, Ph.D and Mgr. Václav Valeš for their assistance with high-temperature X-ray diffraction experiments.

I claim that I have written my work on my own and only with use of the referenced literature. I agree with lending of the thesis and its publication.

In Prague, 13th August 2010 Martin Rusňák

Content

Názov práce: Štruktúrna nespojitosť v hexagonálnych látkach typu RTX

Autor: Bc. Martin Rusňák

Katedra: Katedra fyziky kondenzovaných látok

Vedúci diplomovej práce: RNDr. Jiří Prchal, Ph.D.

e-mail vedúceho: prchal@karlov.mff.cuni.cz

Abstrakt: Ako bolo zistené skôr, kryštálová mriežka ternárnych hexagonálnych *RTX* zlúčenín vykazuje kritikalitu pre špecifické hodnoty pomeru mriežkových parametrov c/a v rozmedzí intervalu 0.565 – 0.575. Aby sme tento efekt preskúmali vo väčšom detaile, pripravili sme polykryštalické vzorčeky $Ce_{1-x}Y_xPdAl$ a SmPdAl a monokryštalické SmPdAl, SmNiAl. V prípade $Ce_{1-x}Y_xPdAl$ došlo k vývoju zakázanej oblasti hodnôt *c/a* v závislosti na kompozícii a teplote. Štruktúrny prechod v tejto sérii nezávisí na teplote. Zlúčenina SmPdAl vykazuje jednofázovosť v celom meranom teplotnom obore napriek tomu, že pomer *c/a* prechádza cez oblasť zakázaných hodnôt. Preukázala sa však prítomnosť kritikality na teplote okolo 500 K. Anomália viditeľná na magnetických a transportných vlastnostiach, ktorá je spojená so zmenou štruktúry, bola nájdená na približne tej istej teplote. Je ponúkané vysvetlenie súvisiace so zvýšeným tepelným pohybom atómov. Popritom, boli vykonané aj magnetické merania v nízkych teplotách. Bola zistená teplota magnetického usporiadania T_c = 15.3 a dominantné antiferromagnetické usporiadanie. Monokryštalický SmNiAl vykazuje správanie veľmi podobné zlúčenine SmPdAl.

Kľúčové slová: RTX; hexagonálna štruktúra typu ZrNiAl; Zakázaná oblasť c/a, Röntgenová difrakcia

Title: Structure discontinuity in the RTX hexagonal materials

Author: Bc. Martin Rusňák

Department: Department of Condensed Matter Physics

Supervisor: RNDr. Jiří Prchal, Ph.D.

Supervisor's e-mail address: prchal@karlov.mff.cuni.cz

Abstract: As it was discovered earlier the crystal lattice of ternary hexagonal *RTX* compounds exhibits a criticality for specific values of the ratio of the lattice parameters *c/a* around the interval of 0.565 – 0.575. To explore this effect in more detail, we have prepared polycrystalline samples of $Ce_{1-x}Y_xPdAl$ and SmPdAl and monocrystalline SmPdAl, SmNiAl. In case of $Ce_{1-x}Y_xPdAl$ series the forbidden range of *c/a* values was found to evolve with composition and temperature. Structural transformation is temperature independent in these compounds. SmPdAl compound is single-phased in the whole temperature range even though the *c/a* ratio crosses the gap of forbidden values common for other compounds. However a criticality in evolution of *c/a* is present at temperature ≈ 500 K. Anomaly visible on magnetic and transport properties, which is connected with change of structure, was found at approximately the same temperature. Explanation based on enhanced thermal movement of the atoms is proposed. Besides, also magnetic measurements at low temperatures were performed. The magnetic ordering temperature T_c = 15.3 K and dominant antiferromagnetic order was found. Monocrystalline SmNiAl exhibits very similar behaviour to the SmPdAl.

Key-words: RTX; hexagonal ZrNiAl-type structure; Forbidden c/a ratio; X-ray diffraction

1 Motivation, previous results

The ternary *RTX* compounds (where *R* ~ rare-earth element, *T* ~ transition metal, *X* ~ *p*-metal) belong to a large group of 1:1:1 compounds. Quite large part of this-group members crystallizes in the hexagonal ZrNiAl-type structure. These compounds exhibit interesting electronic and magnetic properties.

While investigating these properties ([1-5]) an unusual structural behaviour was observed. Some of the compounds abruptly change their lattice parameters *a* and *c* while their temperature or composition is varied (see Figure 1.1). The transformation from one state into another is connected with area of coexistence of both of the structures. This is visible in the diffraction pattern obtained by the means of X-ray diffraction (XRD) as splitting of the peaks (see Figure 1.2).

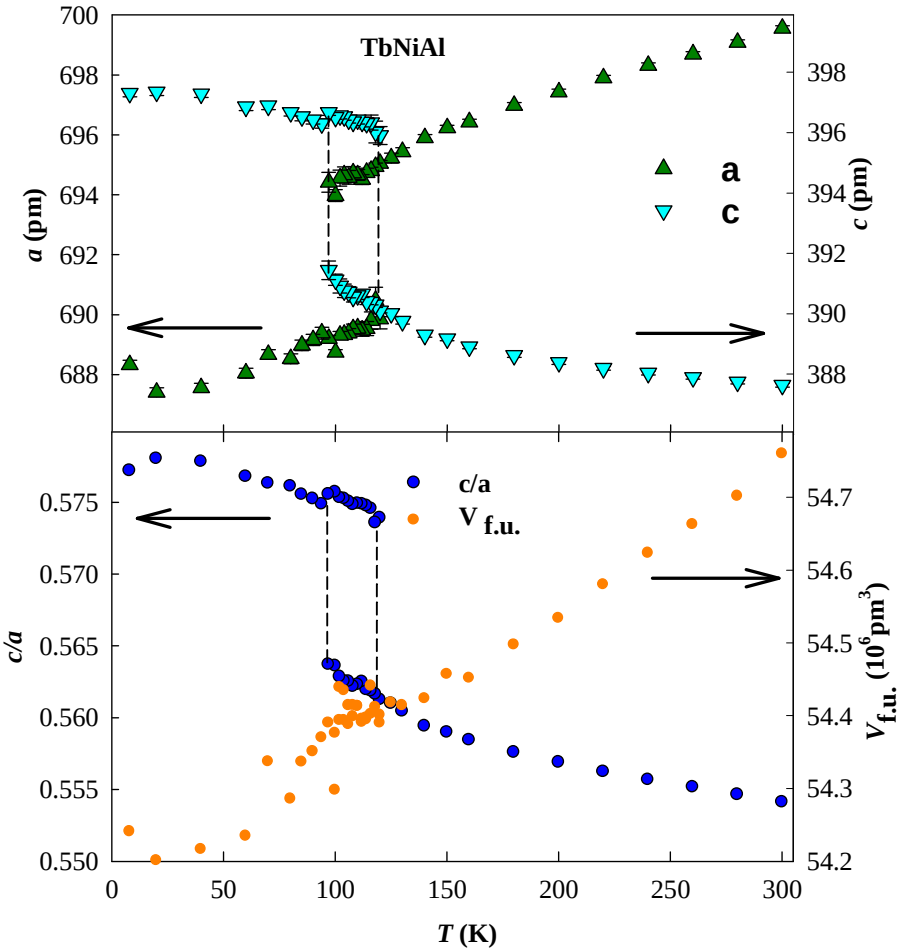

Figure 1.1: Temperature evolution of lattice parameters *a* and *c* of the TbNiAl compound (data taken from [06]). Area of coexistence is delimited by black lines.

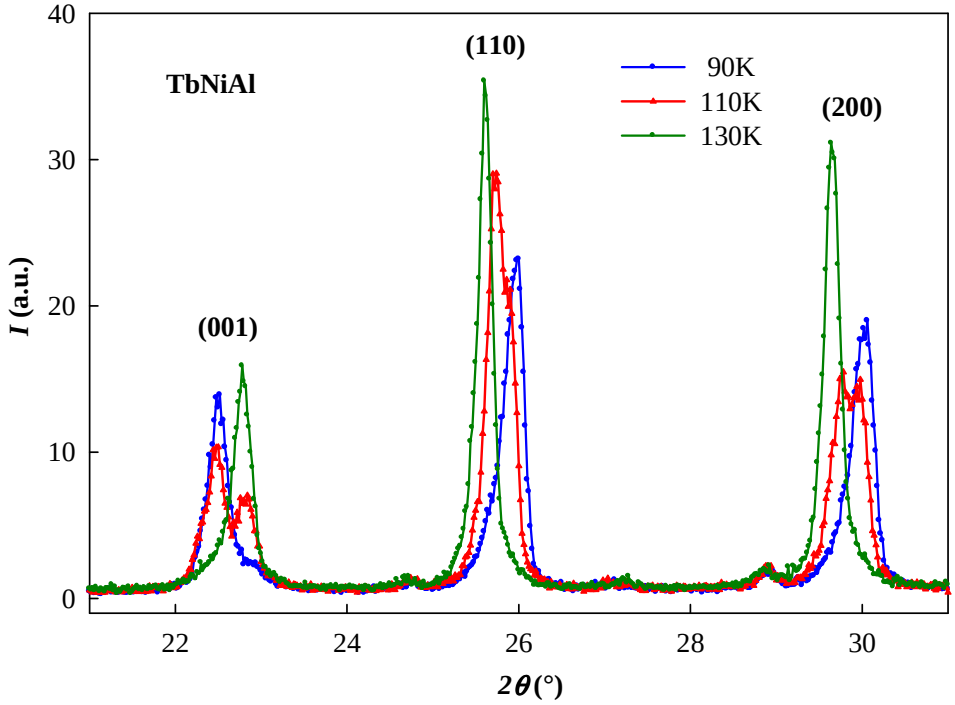

Figure 1.2: Detail of splitted diffraction peaks of the TbNiAl (picture taken from [07]

Depending on the composition of the material, various hexagonal *RTX* compounds embody different absolute values of the lattice constants *a* and *c*, where the abrupt change takes place. Nevertheless, there was found a common feature connecting all these compounds with step-like change of the lattice. The ratio *c/a* skips similar values in all the studied systems, leading to estimation of a "forbidden gap" of the *c/a* ratio between 0.565 to 0.575 (Figure 1.3). In order to call this transformation a phase transition it is necessary that an abrupt change of a state function (in our case Volume) occurs. This does not happen in the compounds where the transformation was observed (see Figure 1.1) Since *a* and *c* exhibit evolution very typical for a 1st order phase transition we will use this term to identify the critical behaviour of *c/a*.

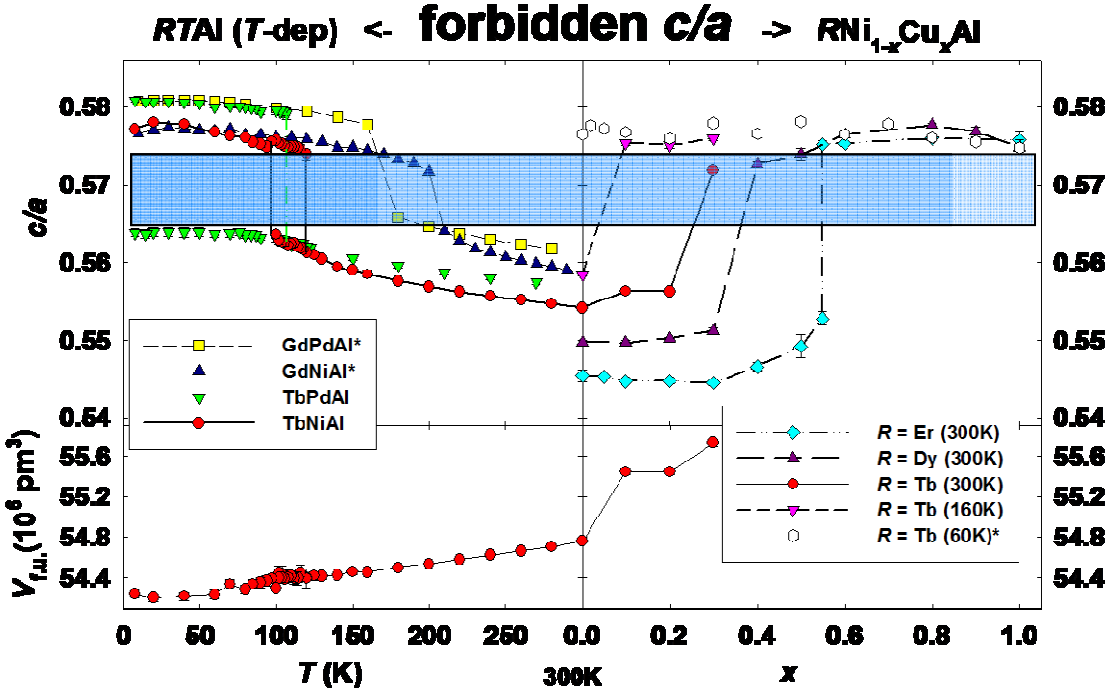

Figure 1.3: The forbidden values of *c/a*. In the bottom part of the picture monotonous evolution of the volume of the formula unit $V_{f.u.}$ is displayed. Figure is taken from [07].

There are different parameters that lead the transformation. Temperature as one of the variables causes such a phase transformation in e.g. GdPdAl [03], GdNiAl [01], TbPdAl [05] , TbNiAl [06].

Another parameter that influences the phase transformation is the composition of the compound while performing a substitution on the *T* position- $RT_{1-x}T_xAl$- takes place in the $ErNi_{1-x}Cu_xAl$ [08] and $DyNi_{1-x}Cu_xAl$ [08]. Study of the substitution on the position of the rare-earth element was performed in $Ce_{1-x}Y_xPdAl$ compounds [09].

Combination of both parameters (temperature and composition) responsible for such a transformation; leading to an interesting possibility to tune the transition temperature; was studied in $TbNi_{1-x}Cu_xAl$ – see the right upper part of Figure 1.3.

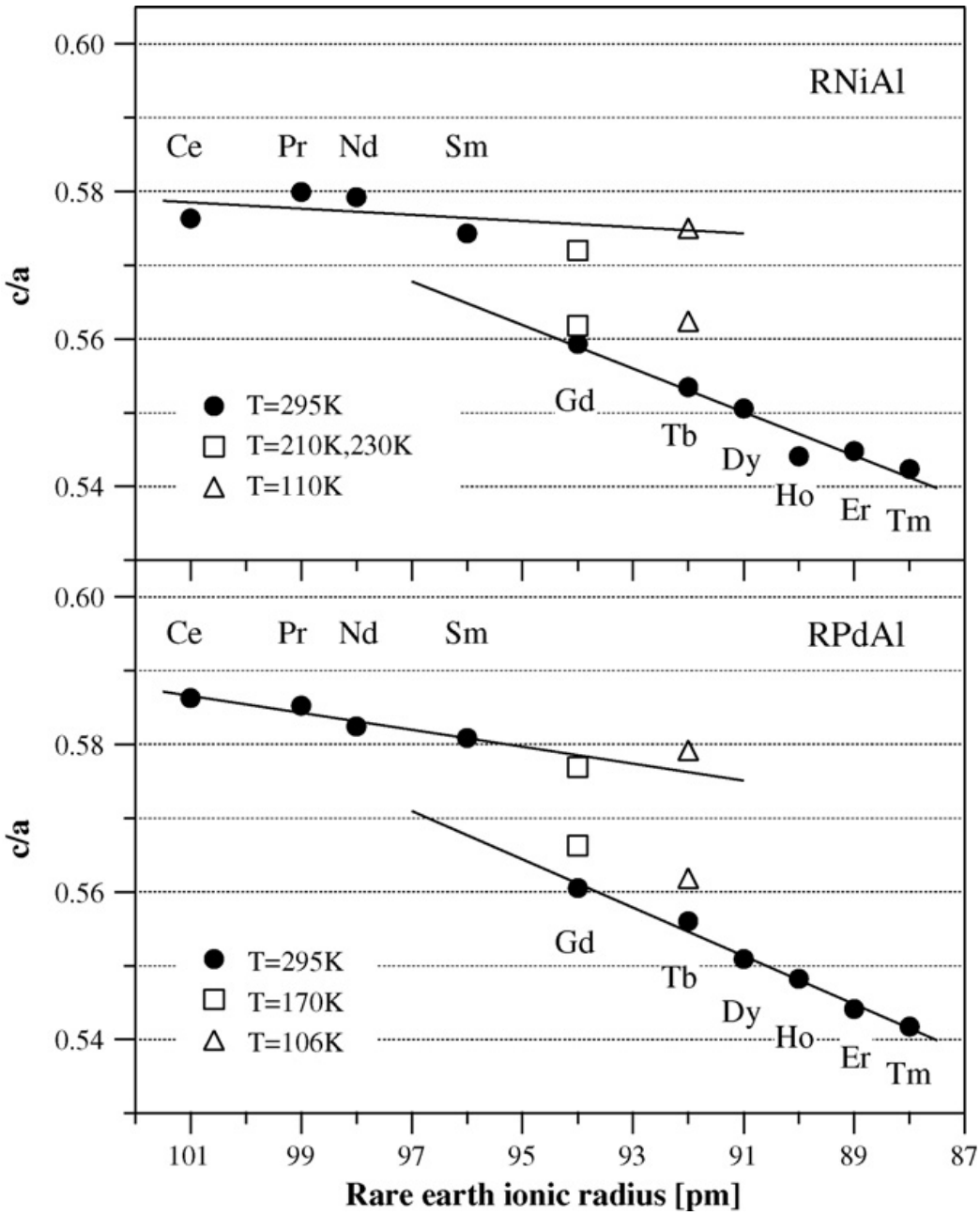

Figure 1.4: Ratio *c*/*a* of hexagonal lattice parameters versus rare-earth (*R*) ionic radius for *R*NiAl and *R*PdAl compounds. Solid lines are a guide to the eye. Figure taken from [10].

Besides the Ce-based series, as the first one with the substitution on the *R*-position exhibiting transformation, another two compounds appeared to occur at the boarder of the critical values of the *c/a* ratio. From the Figure 1.4 one can see that SmNiAl together with SmPdAl exhibit c/a values (at room temperature (RT)) just at the upper edge of the forbidden zone. It is worth to remind that the other systems studied up to now (GdNiAl, GdPdAl, TbNiAl, TbPdAl, ErNiCuAl...) contain rare earth from the second part of the Lanthanides group (the heavy rare-earths), and their c/a is located rather on the bottom

boarder of the forbidden c/a-region (at RT). One can expect that by relatively small deviation from the room temperature will cause similar step-like change from the value above the forbidden gap (let us call it “high c/a”) to the values below the critical values (“low c/a”). Now if we have a look at the Figure 1.5 where the phase diagram of some *R*NiAl compounds is shown, it is possible to notice that the change from low *c/a* into high *c/a* occurs while the temperature is decreased. The border between the phases is highlighted by a green line. By extrapolation of the data it is possible to notice that the border crosses the SmNiAl sample at higher temperatures. Thus we expect the SmNiAl sample to undergo a phase transformation into low *c/a* phase at temperature above the room temperature. RNiAl and RPdAl have similar behaviour (Figure 1.6), therefore SmPdAl compound is expected to undergo a phase transformation as well. These were the reason to perform detailed study on the behaviour of the SmNiAl and SmPdAl at higher temperatures.

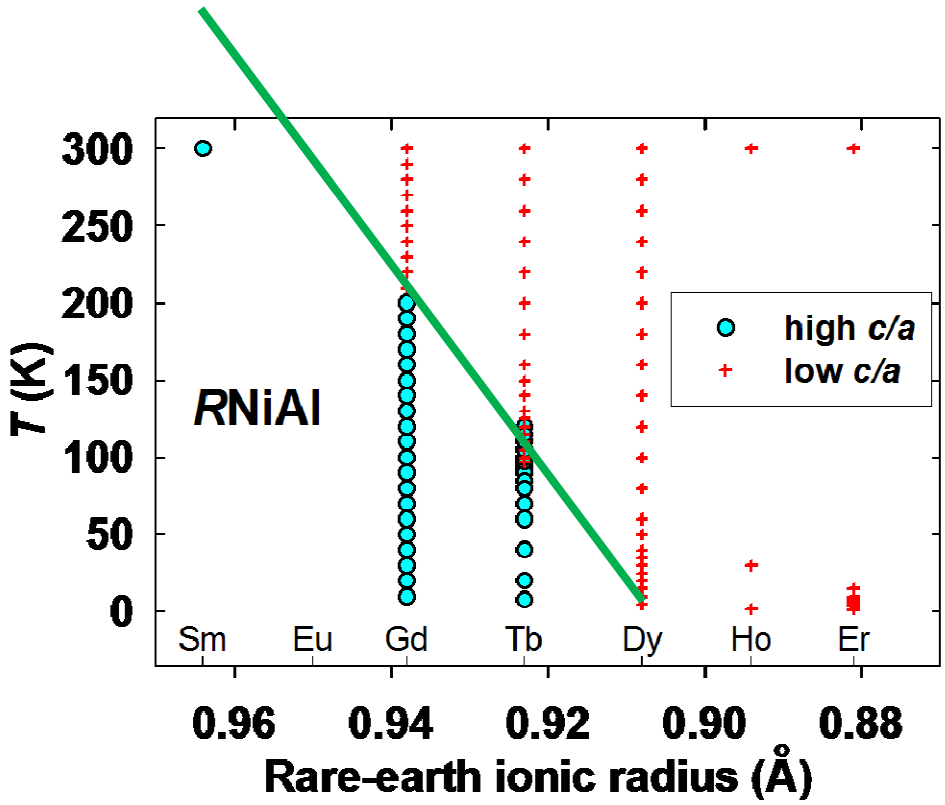

Figure 1.5: Phases diagram of *R*NiAl compounds. The green line represents the border between the high *c/a* and low *c/a* phase. Based on the extrapolated green line one can see that SmNiAl is expected to cross the line and thus undergo a phase transformation at temperatures above the room temperature. Figure is taken from [07].

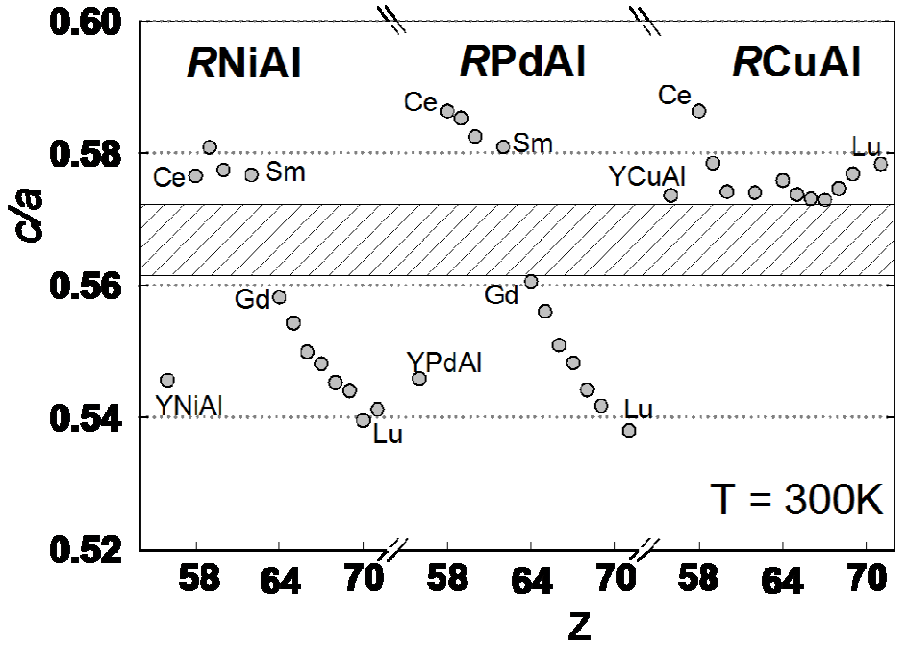

Figure 1.6: Evolution of *c/a* ratio vs. atomic number *Z* of *R* in the *R*NiAl, *R*PdAl and *R*CuAl compounds. Area of forbidden values is marked in the picture. Figure is taken from [07].

2 Theory

2.1 Crystal structure

Crystal structure is a unique arrangement of atoms in a crystal. A crystal structure is made of a motif and a lattice. Motifs are located upon the lattice. Lattice is an array of points periodically repeated in three dimensions. The smallest set of points from which the array can be built and that determine all the symmetry properties of the whole array is called unit cell. The lengths of the edges of a unit cell and the angles between them are called the lattice parameters. Elementary unit may contain more than 1 atom of elements obtained in the structure.

Many of the physical properties such as cleavage, electronic band structure, and optical properties are determined by the structure and symmetry of the crystal. There exist just 230 space groups, depending on the symmetry of the lattice. They can all be built from 14 Bravais lattices (Figure 2.1), that originate from 7 basic lattice types combined with different possibilities of lattice centring.

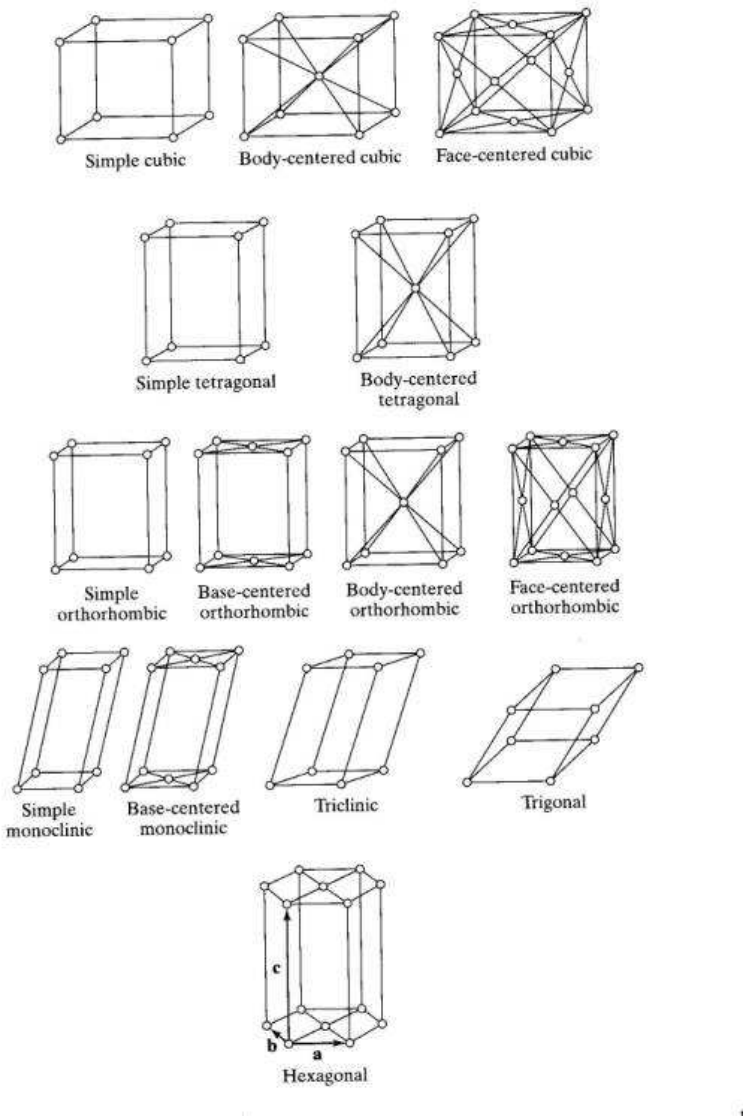

Figure 2.1: Bravais lattice types. Picture taken from [11].

2.2 ZrNiAl-type structure

Our studied materials belong to the group of ternary intermetallic RTX compounds crystallizing in ZrNiAl-type hexagonal structure (space group P-62m; group No. 189; see Figure 2.2).

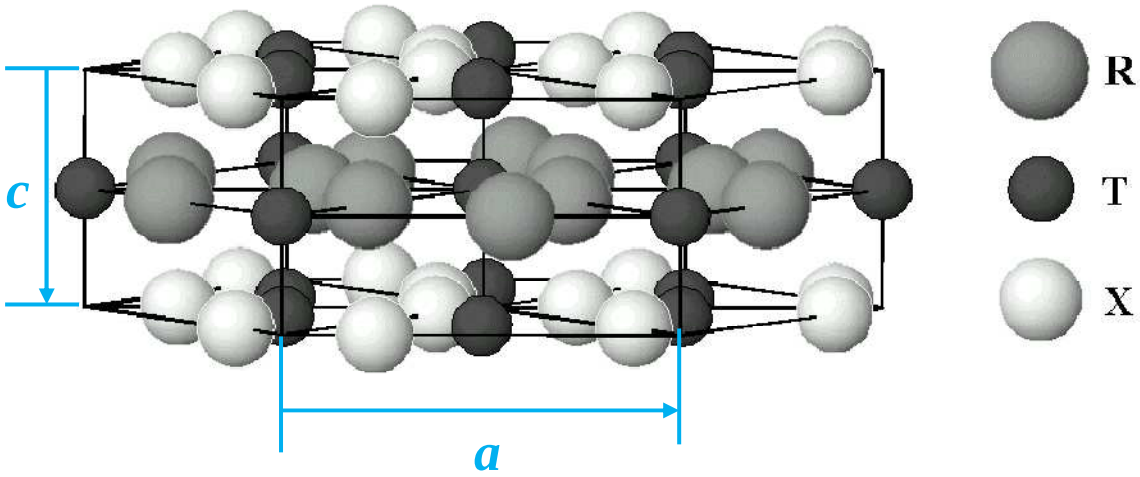

Figure 2.2a): ZrNiAl-type hexagonal structure

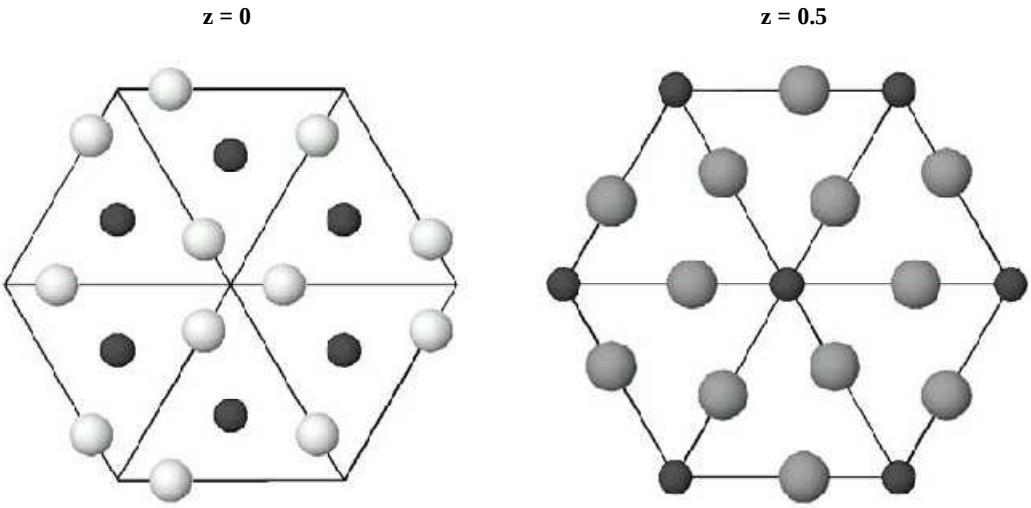

Figure 2.2 b): Two types of basal planes in ZrNiAl-type structure

There are two types of planes in the ZrNiAl-type hexagonal structure (see Figures 2.2.1a, 2.2.1b). One of the basal planes consists of the rare earth atom (R) and one out of three of the transition metal atoms (T). Another (non-magnetic) layer consists of p-metal (X) and two out of the three transition metal atoms (T). These two planes alternate periodically in the ABAB… sequence.

The lattice parameters *a* and *c* are marked in the Figure 2.2. Parameter *a* lies within basal plane. Parameter *c* is perpendicular to the basal plane and connects two planes of the same type. Parameter *b* is sometimes used in hexagonal type of structures; it lies as well within basal plane and is perpendicular to *a*.

The coordinates of the elements are following:

3g (R) : (X_R, 0, ½), (0, X_R, ½), (-X_R, -X_R, ½)

1b (T) : (0, 0, ½)

3f (X) : (X_{Al}, 0, 0), (0, X_{Al}, 0), (-X_{Al}, -X_{Al}, 0)

2c (T) : (⅓, ⅔, 0), (⅔, ⅓, 0)

While the positions of transition-metal atoms are fixed, the positions of rare-earth and p- metal atoms depend on internal structure parameters X_R and X_{Al}.

Volume of the formula unit in the hexagonal type of structures is obtained as:

$$V_{f.u.} = \frac{1}{3} a^2 c . \sin 60° \quad (1)$$

2.3 X-ray scattering

Scattering occurs when X-ray radiation interacts with matter. The interaction of the X-ray radiation with sample can be either elastic or inelastic. Elastic scattering does not involve exchange of the energy between the radiation and sample. It is described by kinematic theory. Inelastic scattering, on the other hand, involves energy transformation and therefore dynamic theory has to be used. In all of our experiments we used elastic scattering.

When incident radiation interacts with matter it gives rise to scattered waves. If the matter is periodically arranged, scattered waves superpose coherently with periodical structure of the sample and give rise to diffracted intensities in specific directions. Method working on this principe is called X-ray diffraction (XRD) and it is mostly used for determining microscopic properties of the matter.

The positions of the diffraction peaks are determined by the Bragg's law of diffraction:

$$\lambda = 2 d_{hkl} \sin\theta \quad (2)$$

Where λ stands for wavelength, d_{hkl} is the distance of reflecting inter atomic planes and θ is the angle between the incident ray and reflecting plane *hkl*.

The intensities of the diffracted peaks are proportional to the square of structure factor F_{hkl}:

$$I \approx |F_{hkl}|^2 \quad (3)$$

Here F_{hkl} is the structure factor and is given by:

$$F = \sum_i f_{at}(q) e^{-2\pi i q r_i} e^{-W_i} \quad (4)$$

The summation is over the elementary cell, $f_{at}(q)$ is the atomic dispersion factor. It is given as a Fourier transformation of the electronic density of the atom. q is the reciprocal space vector. Last term e^{-W_i} is the square root of Debeye-Waller factor; it involves displacement of atoms from their equilibrium position because of thermal movement.

2.4 Magnetism

Magnetic properties of the rare-earth elements depend on their electronic configuration, which can be written as:

$[Xe]\ 6s^2 5d^1 4f^N$

Only the 4f electrons are responsible for the magnetic behaviour of the rare earth ions. Therefore it is important how the electronic 4f shells are filled. In the ground energy state of the atom the filling of the shells follows Hund's rules while obeying Pauli exclusion principle:

1) Electrons arrange so as to maximize spin *S*.
2) While maintaining the first rule the electrons maximize their angular momentum *L*.
3) The total angular momentum is found using $J = |L - S|$ if the shell is less than half full and $J = L + S$ if it is more than half full.

The effective magnetic moment of the ground state is then given by the expression:

$$\mu_{eff} = -\mu_B g_j J \quad (5)$$

Where the parameter g_j is called the Landé factor and can be obtained as:

$$g_j = 1 + \frac{J(J+1)+S(S+1)-L(L+1)}{2J(J+1)} \quad (6)$$

Long range order resulting in magnetic structure in the compounds is provided by exchange interactions. The two basic types of interactions are the direct and indirect exchange (see Figure 2.3).

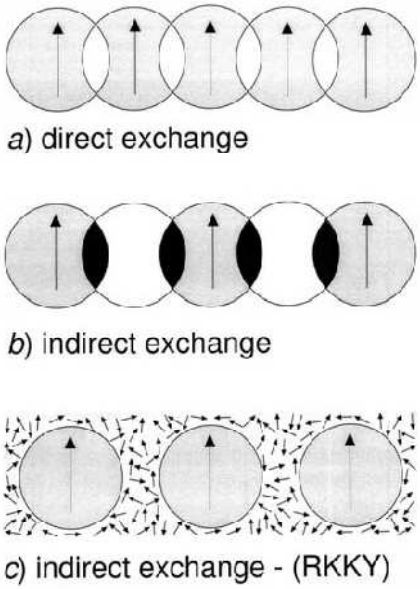

Figure 2.3: Types of exchange interactions in solids.

In the case of rare-earths the direct overlap of 4f electrons' wave functions is negligible. Therefore only indirect interaction will be taken into account.

In *RT*Al compounds, as well as in many other rare-earth based intermetalics, the indirect RKKY exchange type plays significant role. The interaction between magnetic ions is provided by spin-polarised conduction electrons. Taking into account the properties of the conducting electrons, the interaction is of long range and oscillates in dependence on the distance from the original magnetic ion. Therefore abrupt change of the lattice parameters, i.e. distances between the atoms, may cause changes in the magnetic behaviour.

At temperatures below critical temperature T_c, the moments can be aligned by the internal molecular field, even without any applied field being present. Various ground magnetic states may be produced by exchange interactions. Basic types of magnetic structure are

ferromagnetism, antiferromagnetism. In case of ferromagnet all the magnetic moments have parallel alignment. In antiferromagnet magnetic moments lie in antiparallel alignment. At temperatures above T_c the magnetisation of both of these ground magnetic states exhibits paramagnetic character. This behaviour can be described by Curie-Weiss law:

$$\chi = \frac{M}{H} = \frac{\mathrm{N_A}\mu_0\mu_\mathrm{B}^2\mu_{eff}^2}{3\mathrm{k_B}(T-\theta_p)} \quad (7)$$

where χ is magnetic susceptibility, N_A Avogadro constant, μ_0 permeability of vacuum, μ_B Bohr magneton, k_B Boltzmann constant, M magnetisation of the sample, H intensity of applied magnetic field, T temperature and θ_p is paramagnetic Curie temperature.

If the behaviour is not only paramagnetic, but contribution from other types of magnetic interactions (e.g. diamagnetism) has to be used, modified Curie-Weiss law is used to describe the character of sample magnetisation:

$$\chi_M = \chi + \chi_0 \quad (8)$$

3 Experimental methods

3.1 Preparation of the samples

The exact amounts of the elements were prepared according to the stoichiometric ratio of the resulting compounds.

The purity of the elements used was as following:

Al – 5 N (5N means that the given mass contains at least 99.999 % atoms of the requested element – in this case Al)

Ce – 3N

Ni – 4N5 (4N5 means at least 99.995 % atoms of Ni in the given mass)

Pd – 3N in case of the $Ce_{1-x}Y_xPdAl$ compounds
3N5 in case of the SmNiAl and SmPdAl compounds

Sm – SSE (SSE means that the element was purified by the means of solid state electrotransport method. 4N quality is estimated.)

Y- 3N

3.1.1 Polycrystalline samples

The initial mixtures were melted by the mono-arc furnace, installed at Department of Condensed Matter Physics (DCMP), under the protection of an Ar atmosphere (6N) at a pressure of 50 kPa after a previous vacuum of 0.5-2 Pa. Each of the samples was melted and turned 5 times to ensure that the samples will be homogenous. After each melting the weight of the sample was checked to verify that there were not any unexpected losses of material.

3.1.2 Monocrystalline samples

The monocrystalline compounds were grown using modified Czochralski method. In this process ingot grows on seed rod. In the beginning the seed is dipped into melt consisting of materials of the desired crystal. Then the rod is pulled upwards and rotated at the same

time. At this point the ingot may be in polycrystalline form. To obtain monocrystalline compound only one grain is selected. This is done by narrowing of the ingot. Afterwards this grain is propagated into the phase of the resulting ingot. By precisely controlling the temperature, rate of pulling and speed of rotation monocrystalline cylindrical ingot is extracted from the melt.

The growth was performed by the tri-arc furnace, installed at DCMP, under the protection of an Ar atmosphere (6N) at a pressure of 50 kPa after a previous vacuum of 0.6 mPa.

3.2 X-ray powder diffraction

The powder diffraction is used to include every possible orientation of the crystallites of the polycrystalline sample.

Powder diffraction data are usually presented as a diffractogram in which the diffracted intensity I is shown as a function of the scattering angle 2θ. Widespread use of powder diffraction is in the identification and characterisation of crystalline solids, each of which produces a distinctive diffraction pattern. Both the positions and the relative integrated intensity of the lines are indicative of a particular phase and material. In multi-phase mixture, the resulting pattern is a superposition of the phase-patterns, allowing us to determine the relative concentration of the phases in the sample.

Room temperature X-ray powder diffraction

Room temperature experiment was realized on the X-ray diffractometer Bruker D8 Advance from Bruker, installed at DCMP. This device is dedicated for experiments at room temperature. The device works with Bragg-Brentano geometry. A glass plate was used as a sample holder.

High- and low-temperature X-ray powder diffraction

The X-ray diffraction experiment at low temperatures was performed using Rigaku diffractometer equipped by a low-temperature chamber, where cooling is provided by a closed-cycle cryocooler; installed at National Institute for Materials Science, Tsukuba.

The high-temperature XRD experiment was performed on an X-Pert Pro MPD diffractometer with a MRI high temperature chamber; installed at Department of Condensed

Matter Physics, Prague. The sample is put on a tantalum heating strip providing one heating option, but a platinum radiant heater is used as a main heating source to ensure good temperature homogeneity.

Both, the sample and sample holder, were covered by a double-layer and single-layer cover for the low-temperature and the high-temperature experiment, respectively. The covers were evacuated to reduce the thermal exchange between the sample and the outer space and to prevent the sample oxidation at enhanced temperatures.

All three above mentioned devices above work with Bragg-Brentano geometry. The radiation was generated by the Cu-type lamp with selected wave-lengths $\lambda(K_{\alpha 1})$=1.5401Å, $\lambda(K_{\alpha 2})$=1.5445Å in all used equipments. The temperature range was 8 K - 300 K, 300 – 1073 K, in the case of low-temperature experiment, high temperature respectively.

Data analysis

Resulting diffraction patterns were analysed by the program FullProf [12]. This software is based on Rietveld method. Description of this method can be found in [13]. Initial knowledge of the structure type is required for the use of Rietveld method. The program then varies requested parameters in order to find best agreement between the measured and calculated profile.

3.3 X-ray diffraction – Laue method

In the Laue method sample is exposed to polychromatic X-ray radiation and a back-scattering Lauegram is obtained. Illustration of this method is showed in Figure 3.1. Orientation of small pieces of the monocrystalline samples was performed using Chirana Micrometa 2 device installed at DCMP. Device Vistascan was used to display obtained diffraction pattern. It was then analysed and necessary changes to the orientation of the sample were made. After having crystal in desired orientation, pieces of specific shapes were cut by wire saw.

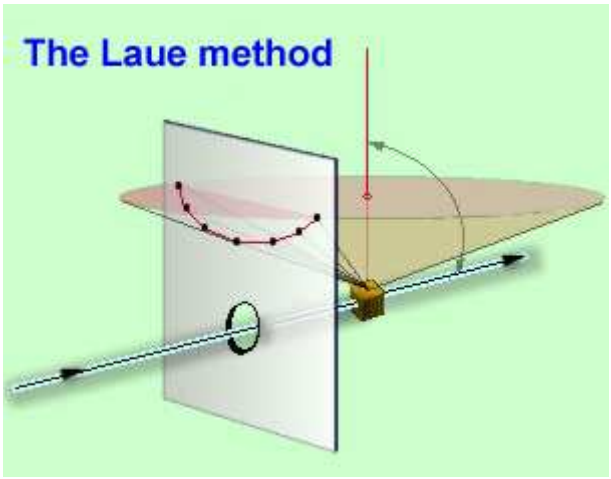

Figure 3.1: Back-scattering Laue method. Arrow marks direction of the beam. Yellow cube represents the sample. White represent plate image plate. Picture taken from [14].

3.4 Magnetisation measurements

Magnetisation measurements were performed on Physical Property Measurement System (PPMS) from the company Quantum design installed at Joint laboratory for magnetic studies. Vibrating Sample Magnetometer (VSM) was used for the measurements. Oven option was installed for the measurement above room temperature. The measurement is accomplished by oscillating the sample near a detection (pickup) coil and simultaneously detecting the voltage induced.

Temperature range was 2 – 570 K. PPMS device allows us to perform measurements in magnetic fields up to 14 T.

3.5 Heat capacity

PPMS instrument with Heat Capacity Measurement System option was used to perform the specific heat experiments. The mass of the samples was around 10 mg. Attachment of the sample to the sample holder was done by Apiezon N grease in order to unsure good thermal contact between the sample and the sampleplate. The two-τ relaxation method is used to determine the heat capacity values. At each measured point a known amount of heating power is applied to the sample. From the temperature evolution the specific heat capacity is calculated.

The measurement is performed at a high vacuum, thus the isobaric heat capacity *Cp* is obtained.

Temperature range was 2 – 385 K. Range of applied magnetic fields was from 0 to 2 T.

3.6 Electric resistivity

Measurements of electric resistivity of the samples were performed using AC Transport Measurement System (ACT) option of the PPMS instrument.

Temperature range was 2 – 300 K. Range of applied magnetic fields was from 0 to 0.5 T.

4 Results and discussion

4.1 $Ce_{1-x}Y_xPdAl$ series

4.1.1 Sample preparation

Five samples with nominal composition x = 0.2, 0.3, 0.4, 0.5, 0.8 ($Ce_{1-x}Y_xPdAl$) were prepared by arc-melting from the initial stoichiometric composition of pure elements in the monoarc furnace as described in part 3.1.

The samples were checked for their quality by X-Ray powder diffraction at room temperature.

All the samples were found to crystallize in the hexagonal ZrNiAl-type of structure. At room temperature the samples with composition x = 0.2, 0.3, 0.8 exhibit single phase diffraction patterns. On the other hand the x = 0.4, 0.5 samples show the coexistence of two different hexagonal phases (see Figure 4.1).

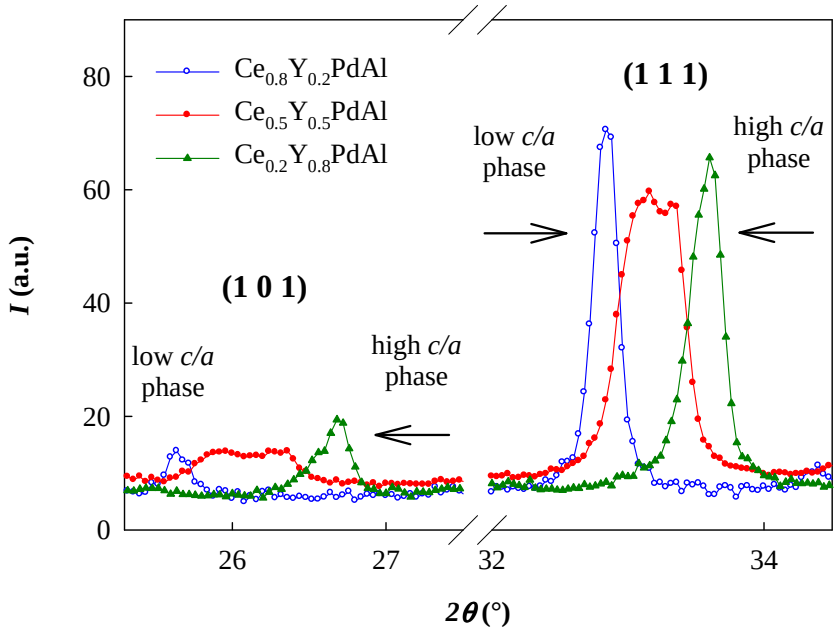

Figure 4.1: Details of the splitting peaks of the $Ce_{0.5}Y_{0.5}PdAl$ sample. The $Ce_{0.8}Y_{0.2}PdAl$ and $Ce_{0.2}Y_{0.8}PdAl$ both exhibit different single phases.

Both of the phases have the same symmetry (ZrNiAl-type), the difference is given by change in values of lattice parameters c and a, in accordance with previous studies at room

temperature [09]. Fitting with this model gives a good agreement as can be seen in Figure 4.2.

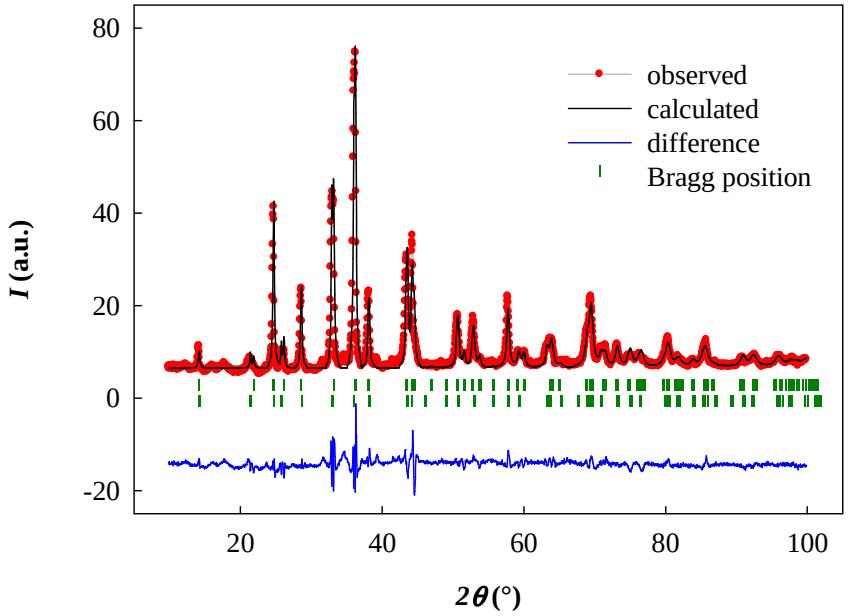

Figure 4.2: Diffraction pattern of $Ce_{0.5}Y_{0.5}PdAl$ compound. The red points represent observed relative intensities, black line is their refinement. One can observe a good agreement between the measured and the calculated profile.

Room temperature values of the lattice parameters *a*, *c*, *c/a* and agreement factor R_{Bragg}, are listed in Table 1.

Table 1: The structural parameters and their uncertainties of the $Ce_{1-x}Y_xPdAl$ compounds at room temperature.

		a(pm)		*c*(pm)		*c/a*		R_{Bragg}
$Ce_{0.8}Y_{0.2}PdAl$		720.17	(0.12)	419.79	(0.09)	0.58290	(22)	14.8
$Ce_{0.7}Y_{0.3}PdAl$		718.18	(0.20)	417.53	(0.14)	0.58140	(35)	13.2
$Ce_{0.6}Y_{0.4}PdAl$	phase 1	718.97	(0.37)	410.28	(0.27)	0.57060	(67)	9.7
	phase 2	718.26	(0.33)	416.81	(0.24)	0.58030	(60)	10.3
$Ce_{0.5}Y_{0.5}PdAl$	phase 1	720.93	(0.36)	406.83	(0.25)	0.56430	(63)	12.3
	phase 2	719.20	(0.45)	414.67	(0.34)	0.57660	(84)	13.1
$Ce_{0.2}Y_{0.8}PdAl$		722.79	(0.50)	397.15	(0.31)	0.54950	(81)	24.0

4.1.2 Structural results

We have studied the $Ce_{1-x}Y_xPdAl$ compounds with x = 0.2, 0.3, 0.4, 0.5, 0.8 by means of low-temperature XRD and, in addition, the samples with x = 0.3, 0.5 were studied by the high-temperature XRD experiment. At temperatures higher than 773 K, the samples undergo an irreversible transformation to unknown, probably amorphous phase, what prevent us from further studies of the ZrNiAl-type phase at higher temperatures.

Structural parameters were obtained using program Fullprof. Temperature dependence of the ratio c/a of the lattice parameters a, c is shown in Table 2 and Figure 4.3.

Table 2 a): The temperature evolution of the ratio of the lattice parameters c/a of the $Ce_{1-x}Y_xPdAl$ compounds with x = 0.2, 0.3 and 0.4 in the temperature range $8 \leq T \leq 773$ K

T (K)	$Ce_{0.8}Y_{0.2}PdAl$		$Ce_{0.7}Y_{0.3}PdAl$		$Ce_{0.6}Y_{0.4}PdAl$			
					phase 1		phase 2	
8	0.58482	(0.41)	0.58305	(0.38)	0.57646	(82)	0.58269	(82)
30	0.58500	(0.39)	0.58325	(0.38)	0.57673	(81)	0.58259	(76)
60	0.58494	(0.37)	0.58363	(0.38)	0.57682	(86)	0.58284	(78)
90	0.58469	(0.38)	0.58329	(0.37)	0.57684	(87)	0.58279	(77)
120	0.58450	(0.36)	0.58299	(0.37)	0.57687	(78)	0.58252	(70)
150	0.58419	(0.35)	0.58290	(0.35)	0.57653	(81)	0.58231	(74)
180	0.58388	(0.31)	0.58268	(0.36)	0.57537	(78)	0.58214	(74)
210	0.58371	(0.34)	0.58244	(0.36)	0.57473	(77)	0.58176	(79)
240	0.58341	(0.32)	0.58212	(0.35)	0.57343	(77)	0.58144	(74)
270	0.58296	(0.28)	0.58185	(0.36)	0.57201	(64)	0.58077	(59)
300	0.58289	(0.22)	0.58138	(0.35)	0.57064	(67)	0.58030	(60)
300			0.5808	(0.12)				
373			0.5800	(0.13)				
473			0.5791	(0.13)				
573			0.5765	(0.13)				
673			0.5756	(0.12)				
773			0.5744	(0.14)				

Table 2 b): The temperature evolution of the ratio of the lattice parameters *c/a* of the $Ce_{1-x}Y_xPdAl$ compounds with $x = 0.5$ and 0.8 in the temperature range $8 \leq T \leq 773$ K

T (K)	$Ce_{0.5}Y_{0.5}PdAl$				$Ce_{0.2}Y_{0.8}PdAl$	
	phase 1		phase 2			
8	0.56808	(0.82)	0.57844	(0.78)	0.55005	(80)
30	0.56840	(0.87)	0.57853	(0.81)	0.55014	(82)
60	0.56869	(0.86)	0.57865	(0.81)	0.55022	(78)
90	0.56873	(0.81)	0.57943	(0.74)	0.55022	(93)
120	0.56807	(0.82)	0.57919	(0.73)	0.55025	(89)
150	0.56768	(0.80)	0.57884	(0.74)	0.55014	(86)
180	0.56738	(0.78)	0.57862	(0.74)	0.55011	(89)
210	0.56640	(0.74)	0.57771	(0.75)	0.55012	(90)
240	0.56586	(0.66)	0.57743	(0.71)	0.54988	(94)
270	0.56573	(0.65)	0.57737	(0.73)	0.54974	(93)
300	0.56432	(0.63)	0.57657	(0.84)	0.54948	(81)
300	0.5649	(0.10)	0.5773	(0.14)		
373	0.5604	(0.12)	0.5714	(0.13)		
473	0.5585	(0.11)	0.5687	(0.12)		
573	0.5578	(0.11)	0.5679	(0.13)		
673	0.5576	(0.09)	0.5676	(0.10)		
773	0.5579	(0.11)	0.5673	(0.13)		

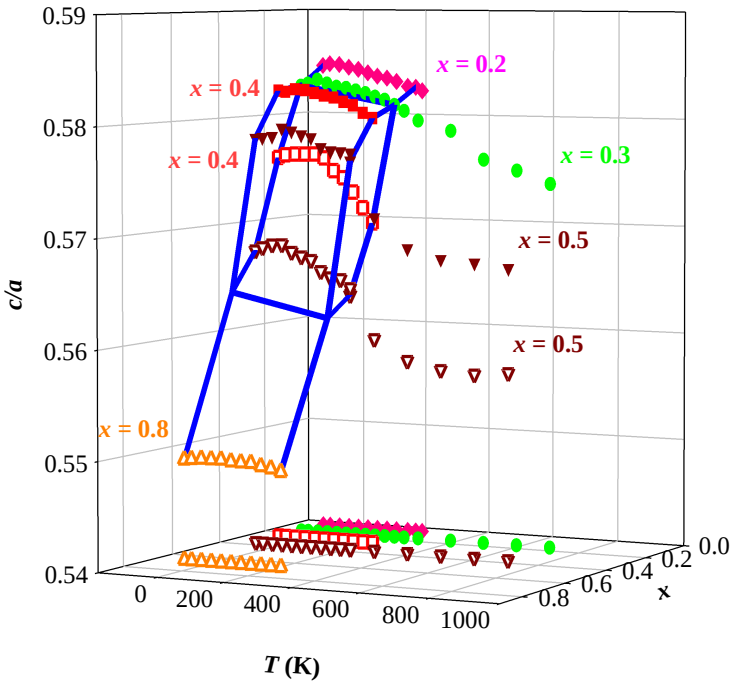

Figure 4.3: The temperature and concentration evolution of the *c/a* ratio of the lattice parameters *a* and *c* of the $Ce_{1-x}Y_xPdAl$ compound. The thick lines set bounds to the zone of forbidden values of *c/a*.

Existence of a forbidden gap was confirmed, whereas in the case of (Ce,Y)PdAl compounds the gap varies in values of *c/a* that are not constant within both - temperature and composition. Varying the Y-concentration parameter from 0 to 1 at room temperature the forbidden gap changes from (0.570-0.579 for $x = 0.4$) to (0.555-0.566 for $x = 0.6$ [09]). For temperature evolution of the sample $x = 0.5$ the critical values of *c/a* can be found in the range from (0.568 - 0.578 for $T = 8$ K) to (0.558 - 0.567 at 773 K). Both – the chemical composition (different atomic radii) and temperature (change of the lattice parameters due to atomic thermal movement) influence the critical values of *c/a* in the $Ce_{1-x}Y_xPdAl$ compounds which form a quasi plane in the phase space.

In contrast to previously studied systems with substitution on transition-metal position, where boundary between lattices of compounds having *c/a* above- and below the forbidden values (0.565 - 0.575) is crossing the "vector of temperature direction" (Figure 1.5), so that the transition can be observed by varying the temperature; in the case of $Ce_{1-x}Y_xPdAl$ the border between the phases is parallel to the temperature direction and position of the boundary is almost temperature independent (see Figure 4.4).

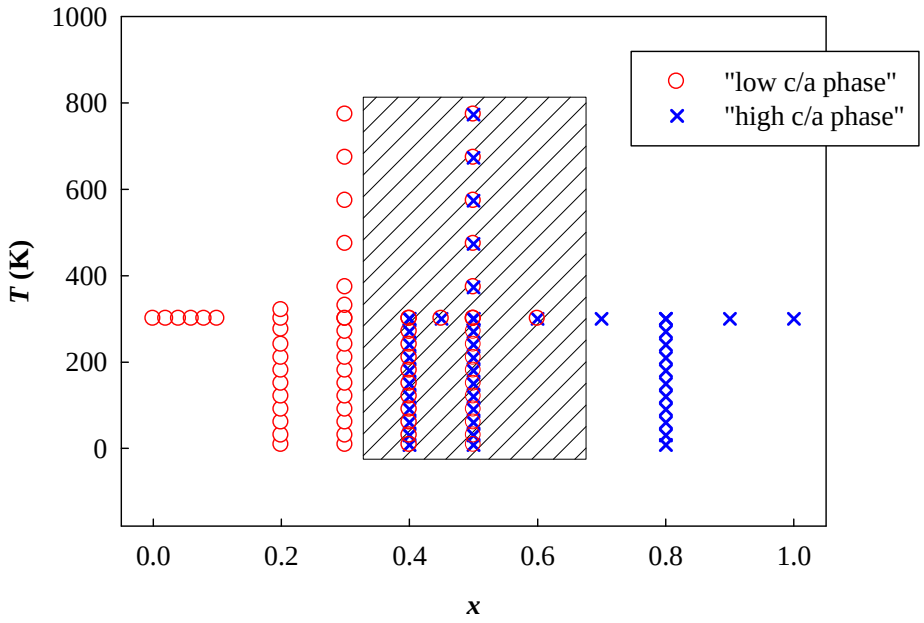

Figure 4.4: The phase diagram for the $Ce_{1-x}Y_xPdAl$ compound. Filled part marks the area of coexistence of both of the phases. It is obvious that border between the phases is parallel to the temperature. Additional data for compounds with x = 0.0 to 0.1 and 0.9 to 1.0 were taken from [09].

The difference between the constant range of forbidden critical values - as in previously studied systems - and temperature- and concentration dependent ranges - as in the present studied system - are caused by the fact that substitution in the $Ce_{1-x}Y_xPdAl$ series is made on the position of the rare-earth element. Since the rare-earth element in the ZrNiAl-type structure is present only in one type of the layers alternating along the *c*-axis (see Figure 2.2 (contrary to the transition metal, which is situated in both types of the layers), thus also the substitution takes place only within one of the two types of layers in $Ce_{1-x}Y_xPdAl$. This is the main difference from the previously studied $RT_{1-x}T'_xAl$ compounds. The R-Pd layer is thus directly affected by the substitution. The Pd-Al layer is affected by the Ce-Y substitution indirectly through the interlayer bonding. Because of conserving the crystallographic symmetry, also after the substitution the lattice parameter *a* has to be equal in both types of the layers. The volume of the unit cell shifts correspondingly to the difference of the volumes of the substituted atoms. In the layered type structure of $Ce_{1-x}Y_xPdAl$ it is more preferred to change the lattice parameter *c*, which is mainly affected by the weaker interlayer bonding, than to vary *a* in the Pd-Al layer, which is mainly bounded by the stronger interplanar bonding (the nearest neighbouring atoms are can be found within the planes). This

leads to the conclusion that the governing parameter for the transition in our case is *c*. This statement is supported by the value of change in *c* compared to the change in *a*. In $Ce_{0.5}Y_{0.5}PdAl$ the parameter *c* increases from 406.83 pm to 414.67 pm at 300 K, i.e. by 2 % what is 7 times more than change in *a*, which at the same point changes from 720.93 pm to 719.20 pm. Contrary to that, in previously studied systems, the relative change of the parameters *a* and *c* was 0.6% and 1%, respectively for TbNiAl at 110 K [06]; also 1.3% in *a* and 2.8% in *c* for $ErNi_{1-x}Cu_xAl$ [08] between $x = 0.5$ and 0.6 at room temperature, what means only about 2-times difference between the changes of the respective lattice parameters. We assume that the different character of the substitution of the compounds is the main reason for the temperature and composition dependence of the forbidden values of the *c/a*.

4.2 SmPdAl, SmNiAl

4.2.1 Sample preparation

4.2.1.1 SmPdAl polycrystalline sample

The SmPdAl sample was prepared using the methods described in chapter 3.1.1. We first set the stoichiometric ratio of Sm : Pd : Al as 1.3 : 1 : 1.03 (notation $Sm_{1.3}Pd_1Al_1$-poly will be used), even thought the desired sample composition was 1:1:1. Higher amount of Sm was added because of its higher evaporation compared to the other two elements. Temperature dependency of vapour pressure *p* of all the elements used is shown in Figure 4.5.

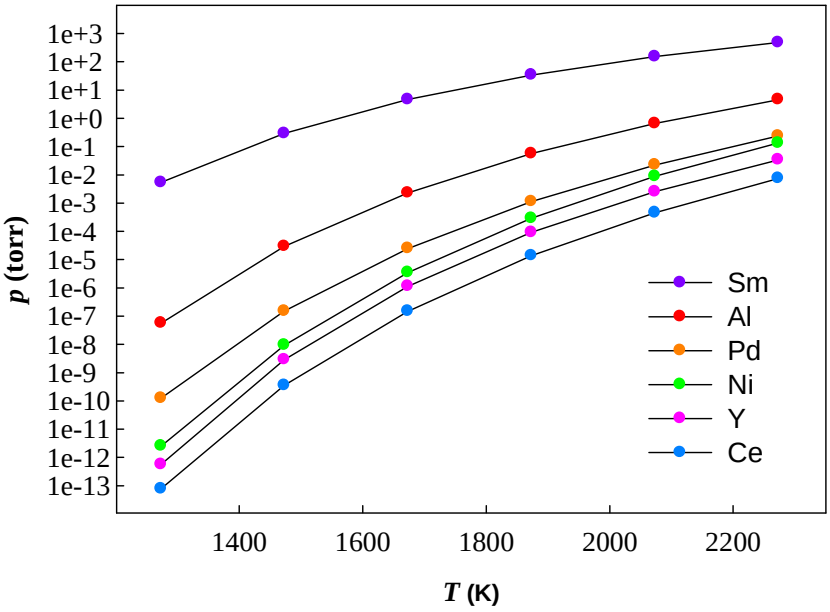

Figure 4.5: Vapour pressure of the Sm, Al, Pd, Ni, Y and Ce elements in dependency on temperature.

Having the sample prepared, microprobe and X-ray powder diffraction measurements were performed. XRD measurement showed that the sample crystallises in desired hexagonal ZrNiAl-type structure. On the other hand there was another impurity phase present, as can be seen in Figure 4.6. Electron microprobe experiment identified this phase as mainly consisting of Samarium (Figure 4.7 and Table 3).

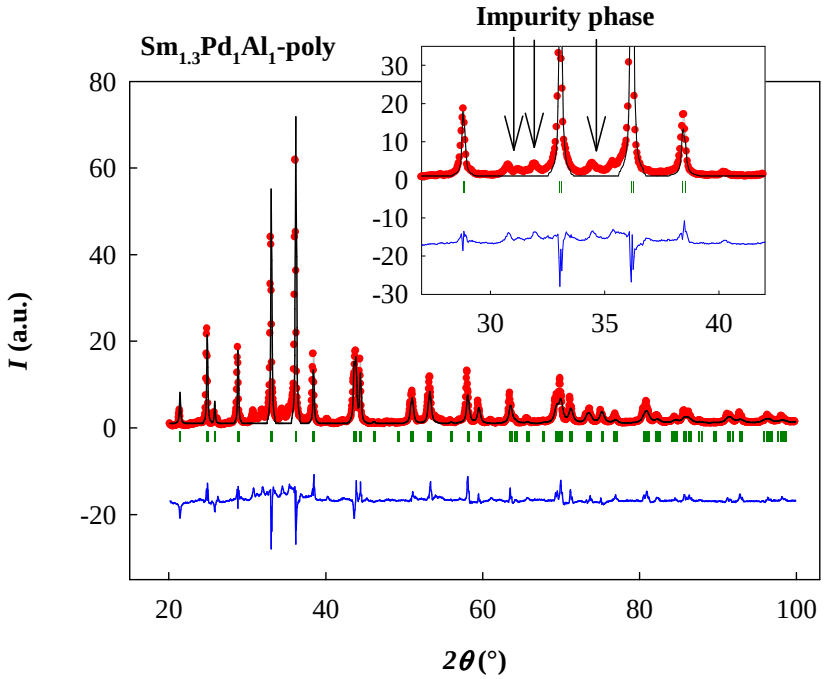

Figure 4.6: Diffraction pattern of $Sm_{1.3}Pd_1Al_1$. The red points represent observed relative intensities; black line is their refinement; blue line is difference between them and green vertical lines represent the calculated Bragg position. Reflections from impurity phases can be observed.

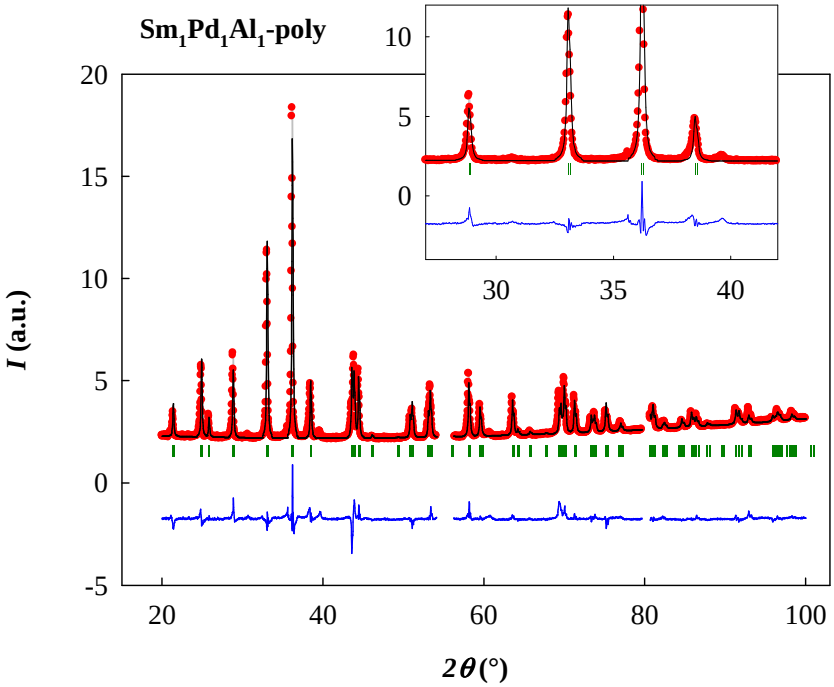

Figure 4.8: Diffraction pattern of $Sm_1Pd_1Al_1$ polycrystalline compound. The red points represent observed relative intensities, black line is their refinement. One can observe a good agreement between the measured and the calculated profile.

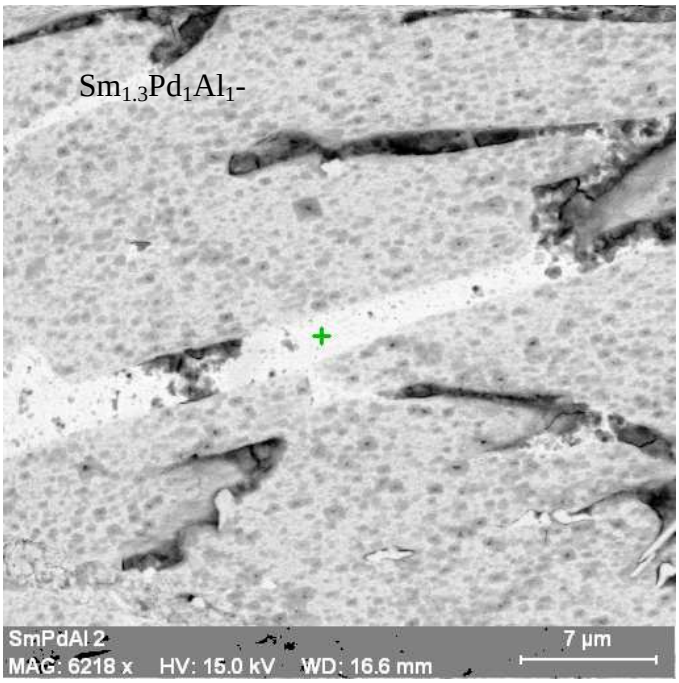

Figure 4.7: Picture of the $Sm_{1.3}Pd_1Al_1$ polycrystalline sample from electron microprobe experiment. Green cross marks area where the current measurement is being performed. Currently it is focused on a phase rich on Sm - the white path.

Table 3: Concentration of the Samarium-rich phase in comparison to the main phase in $Sm_{1.3}Pd_1Al_1$-polycrystalline compound

Element	Relative concentration (%)	
	Sm-rich phase	Main phase
Sm	57.8 (2.2)	36.2 (1.6)
Al	21.1 (0.3)	33.5 (0.6)
Pd	21.0 (0.6)	30.2 (0.2)

This brought us to the idea that Sm once becoming part of the SmPdAl compound does not evaporate so much. Based on this experience, the initial stoichiometric ratio used for the next preparation step was Sm = 1.03, Pd = 1.00, Al = 1.03 (notation- $Sm_1Pd_1Al_1$-poly). The small extra amount of Sm and Al is added since the evaporation of Sm is not as significant as thought but still higher than evaporation of Pd (see Figure 4.5). The same reason applies for Al. At this stage polycrystalline sample was prepared. Again electron microprobe (Table 4) and X-ray powder diffraction measurements (Figure 4.8) were performed and stated that sample is of a high quality and the impurity phases are much less populated than in the case of $Sm_{1.3}Pd_1Al_1$-poly, as can be observed from comparing of the focused parts in Figures 4.6 and 4.8.

Table 4: Elements concentration in the main phase of the $Sm_1Pd_1Al_1$-polycrystalline compound

Element	Relative concentration (%)
Sm	33.3 (1.6)
Al	29.9 (0.6)
Pd	36.9 (0.3)

4.2.1.2 SmPdAl monocrystalline sample

The experience gained in the process of preparing SmNiAl monocrystalline sample, led us to the initial stoichiometric ratio of Sm : Pd : Al as following 1.03 : 1 : 1.03 (notation-SmPdAl-mono).

The initial mixtures were first 2 times melted using the mono-arc furnace and afterwards used as initial compound in the tri-arc furnace. Monocrystalline sample of SmPdAl was successfully prepared. Quality and crystal structure was checked using powder XRD and proved that the sample crystallised in ZrNiAl-type structure and that is of high quality as one can observe from Figures 4.9 and 4.10 b).

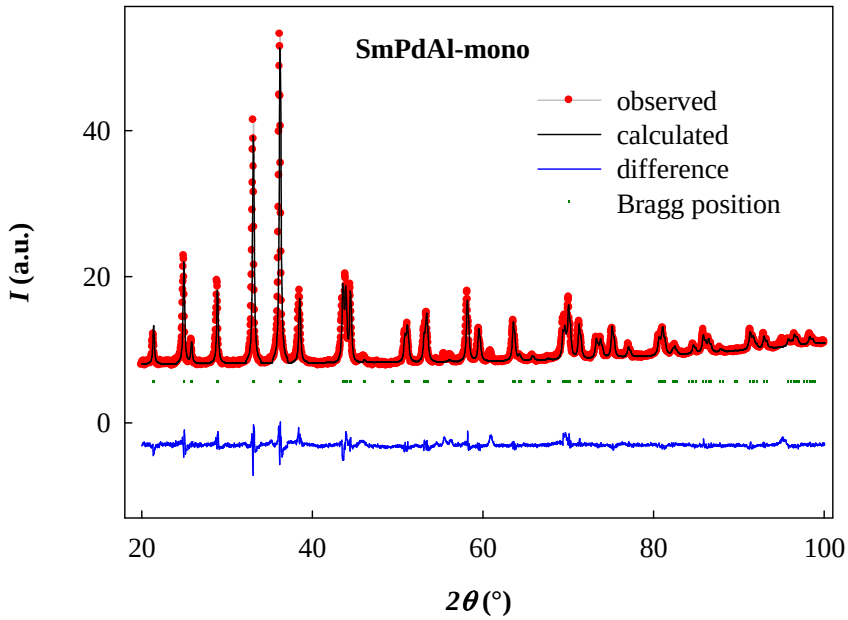

Figure 4.9: Diffraction pattern of SmPdAl monocrystalline compound.

Monocrystalline compounds are in general of a higher quality compared to the polycrystalline ones. In Figure 4.10 to compare SmPdAl samples either in poly or

monocrystalline form the details of diffraction patterns of both of the samples are displayed. One can notice that the quality of SmPdAl-mono is better than the one of the polycrystalline compound since the impurity phases visible in the poly-sample cannot be found in the mono-compound.

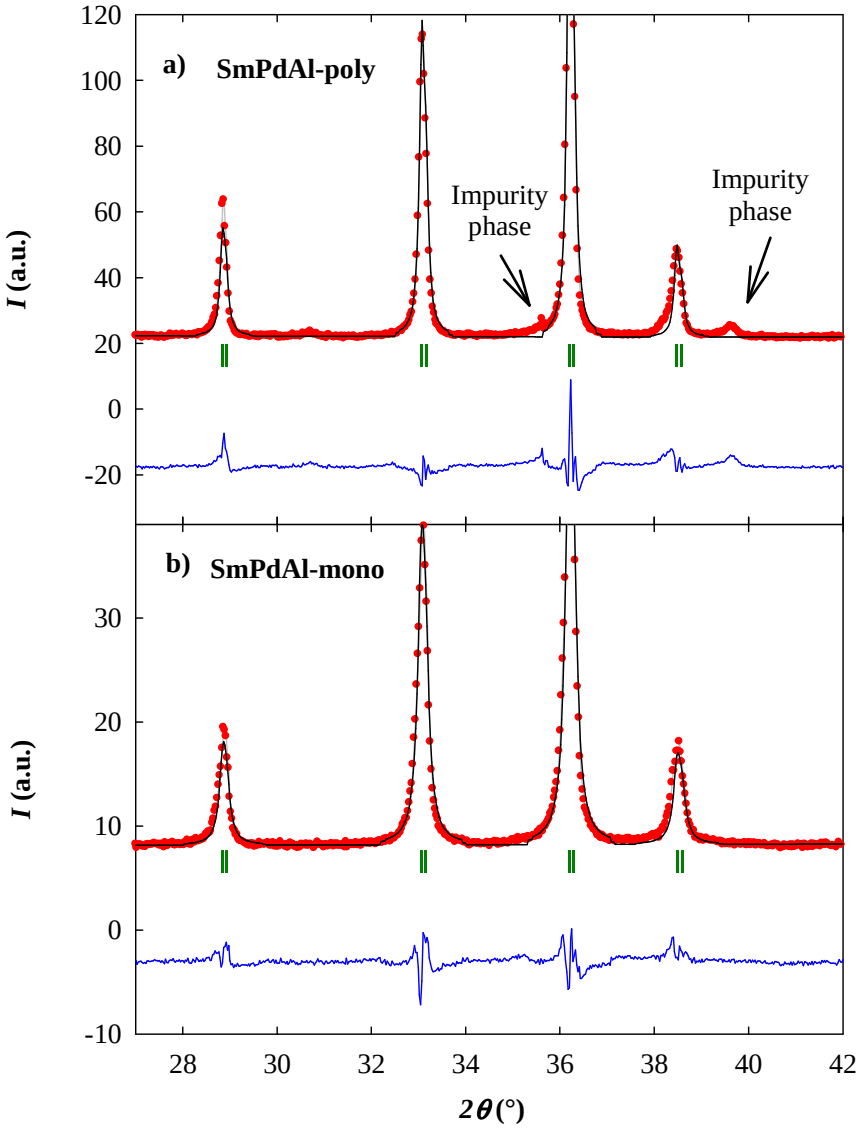

Figure 4.10: Comparison of diffraction patterns of SmPdAl poly- and monocrystalline samples. The red points represent observed relative intensities, black line is their refinement. Impurity phases that are present in the polycrystal are not present in the monocrystalline sample.

Smaller pieces with known orientation with respect to the specific crystallographic directions of the crystal were prepared. The orientation was performed using Micrometa (see chapter 3.2). Afterwards the pieces were cut using wire saw. The pieces were oriented in two

main directions; along the hexagonal *c*-axis and perpendicular to it (within basal (a, b)-plane). Lauegram of the crystal oriented with *c*-axis perpendicular to the plane of film is shown in Figure 4.11.

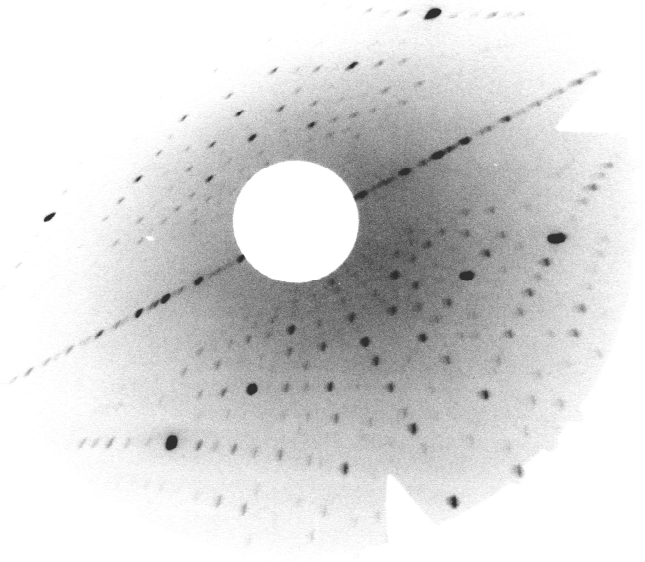

Figure 4.11: Lauegram of the monocrystalline SmPdAl. Reflection (100) is situated in the centre.

4.2.1.3 SmNiAl polycrystalline sample

The sample of polycrystalline SmNiAl compound (notation SmNiAl-poly) was already prepared during previous studies in the DCMP. We checked the quality of the sample using XRD. Diffraction pattern together with calculated intensity and their difference is shown in the following Figure 4.12. The measured and calculated profiles are in a very good agreement.

SmNiAl polycrystalline sample was found to consist of two-phases at room temperature. Both of them form the hexagonal ZrNiAl-type structure. One of the phases is the high *c/a* phase the other one is the low *c/a*. Details of the peaks splitting connected with this phenomena are displayed in Figure 4.13.

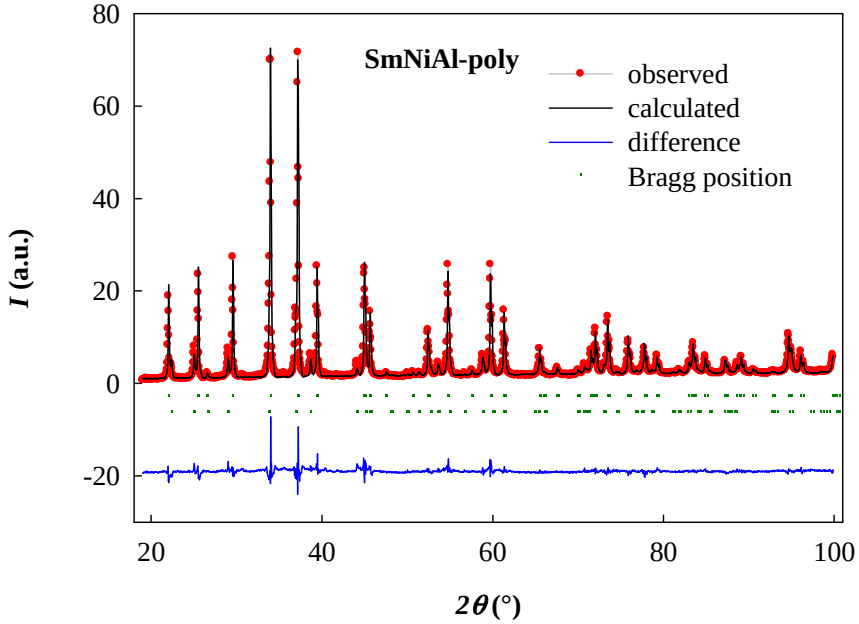

Figure 4.12: Diffraction pattern of SmNiAl polycrystalline sample.

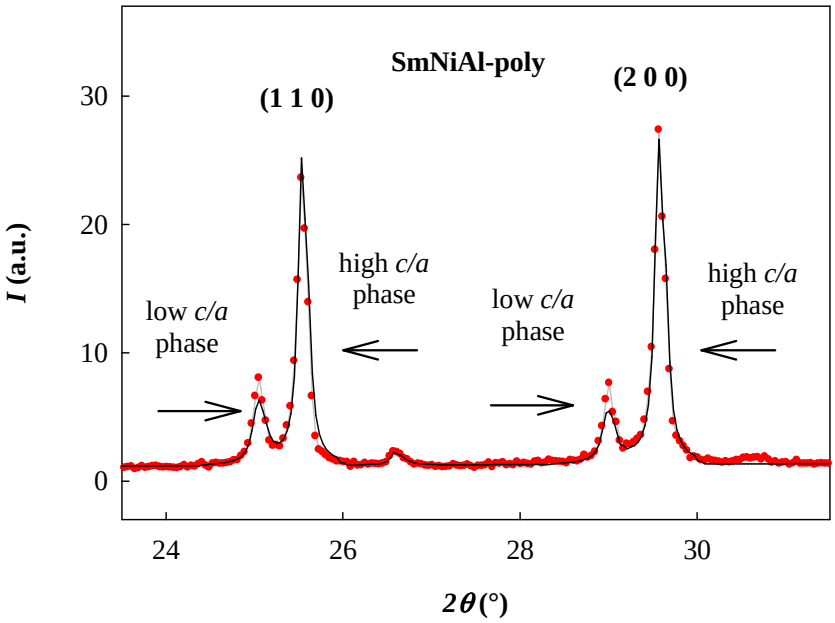

Figure 4.13: Detail on the splitting of the peaks of the SmNiAl polycrystalline sample. Red points represent measured intensity, black lines calculated intensities and the numbers in brackets mark reflexion types.

4.2.1.4 SmNiAl monocrystalline sample

SmNiAl monocrystalline sample was prepared using tri-arc furnace as described in section 3.1.2. We already knew that Sm does not evaporate as much in this type of compounds. Nevertheless, mainly because the melting in mono-arc furnace takes only few second or a minute and the growth of crystal in the mono-arc furnace is a process which takes some hours, we decided to use stoichiometric ratio of Sm : Ni : Al as 1.3 : 1 : 1.03 for the first set. Notation $Sm_{1.3}Ni_1Al_1$-mono will be used in this case.

Elements were placed in the furnace and using Czochralski method (chapter 3.1.2) we succeeded in preparing an ingot.

X-ray powder diffraction was performed on the crystalline sample. The compound appeared to crystallize in the requested hexagonal ZrNiAl-type of structure, however presence of impurity phases was observed (see Figure 4.14 for the diffraction pattern and Figure 4.15 a) for its detail).

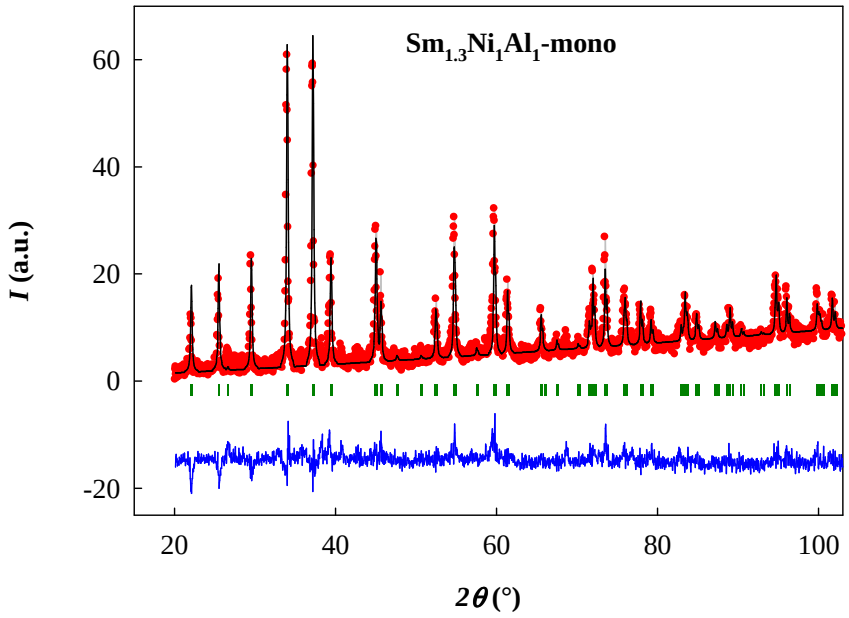

Figure 4.14: Diffraction pattern of the $Sm_{1.3}Ni_1Al_1$-monocrystalline sample.

Phase analysis using electron microprobe experiment revealed that the preparation of monocrystalline sample was not successful since the sample crystallised in a polycrystalline form. Phase with highest population – dark grey in the Figure 4.16 and dark grey marked with green dot in Figure 4.17 has stoichiometric ratio corresponding to the SmNiAl in stoichiometric ratio 1:1:1 as can be seen from the results in the Table 5.

Other two phases, which are not populated so much, contain more Sm- Sm and Ni respectively (again, see Figures 4.15, 4.16 and Table 5).

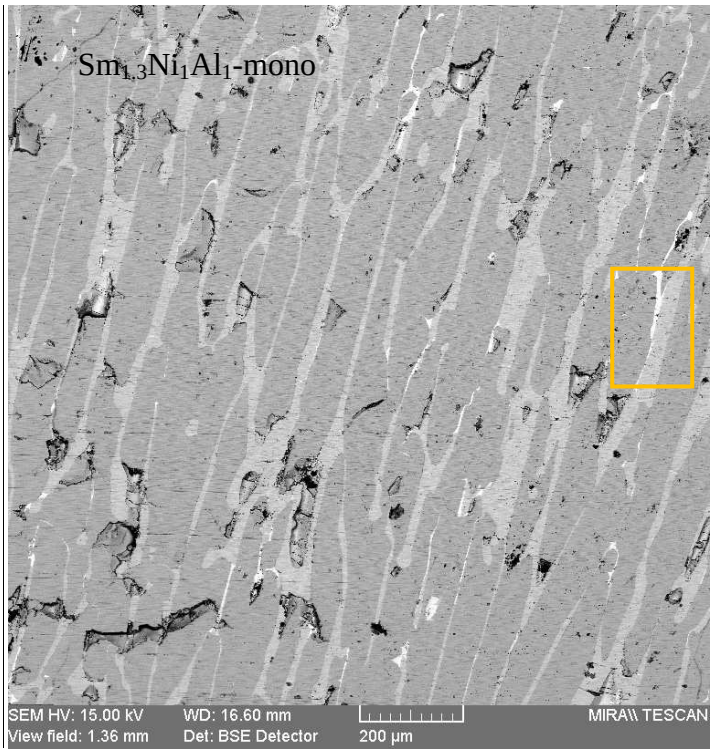

Figure 4.16: Picture from the electron microprobe phase analysis of the $Sm_{1.3}Ni_1Al_1$ compound. Area where the analysis was performed is highlighted by a yellow rectangle.

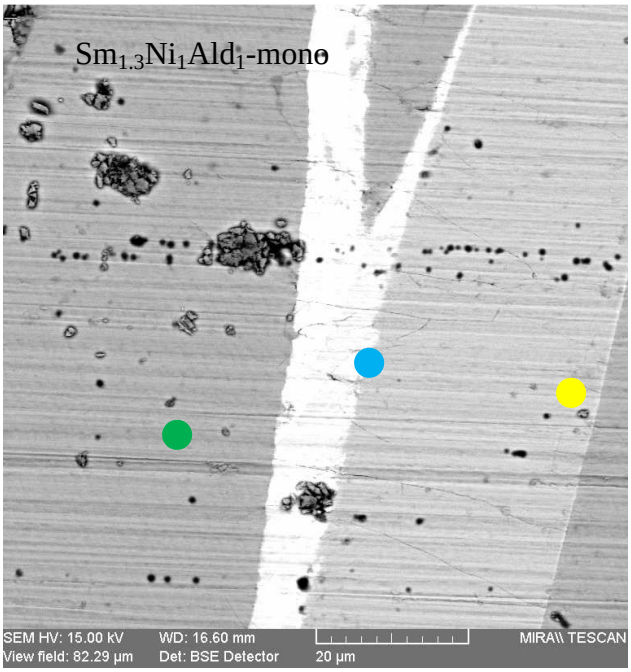

Figure 4.17: Area where the electron microprobe analysis on the $Sm_{1.3}Ni_1Al_1$ sample was performed. Three different phases are to be seen, each is marked by a colourful dot.

Table 5: Concentration of the elements in different phases of the $Sm_{1.3}Ni_1Al_1$-mono sample. Dots correspond to the marks displayed in Figure 4.17.

Relative concentration (%)					
Element	Phase 1		Phase 2		Phase 3	
Sm	31.2	(2.3)	64.7	(3.1)	37.6	(2.5)
Ni	35.1	(8.4)	21.2	(5.9)	41.7	(8.7)
Al	33.5	(0.7)	13.9	(0.2)	20.5	(0.4)

According to the results obtained while preparing the first sample for the next set - $Sm_1Ni_1Al_1$-mono - stoichiometric ratio Sm = 1.03, Ni = 1.00, Al = 1.03 was chosen. Reason for a little bit higher concentration of Sm and Al is described in SmPdAl polycrystalline sample preparation (section 4.2.1).

The initial mixtures were first 2 times melted using the mono-arc furnace. This was performed to ensure homogenous distribution f the elements over the whole volume of the melt as good as possible.

The compound created in mono-arc furnace was used as initial for the crystal growth in the tri-arc furnace by using Czochralski method we succeeded to grow a crystal. Using X-Ray powder diffraction quality was checked. The phase quality was checked by the Laue method (Chapter 3.3). The crystal was found to be monocrystalline and having the ZrNiAl-type structure. The diffraction pattern together with calculated intensity and their difference is shown in Figure 4.18. Quality and phase purity of $Sm_1Ni_1Al_1$ in comparison to $Sm_{1.3}Ni_1Al_1$ is demonstrated in Figure 4.15.

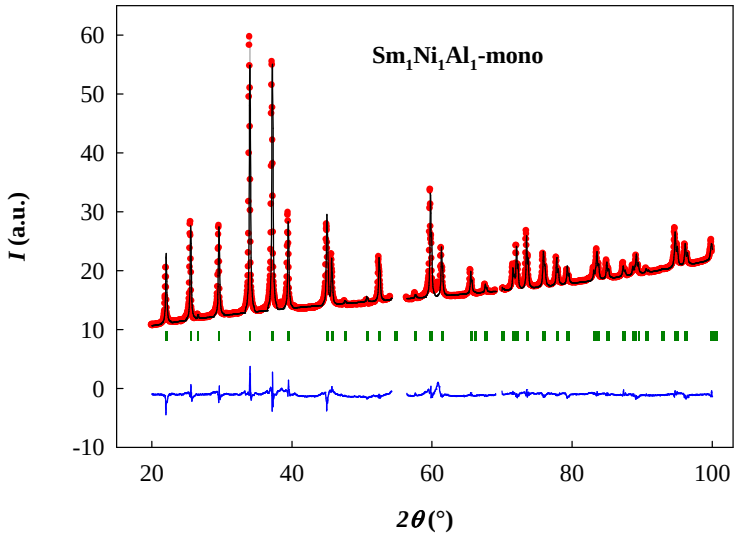

Figure 4.18: Diffraction pattern of the $Sm_1Ni_1Al_1$-monocrystalline sample.

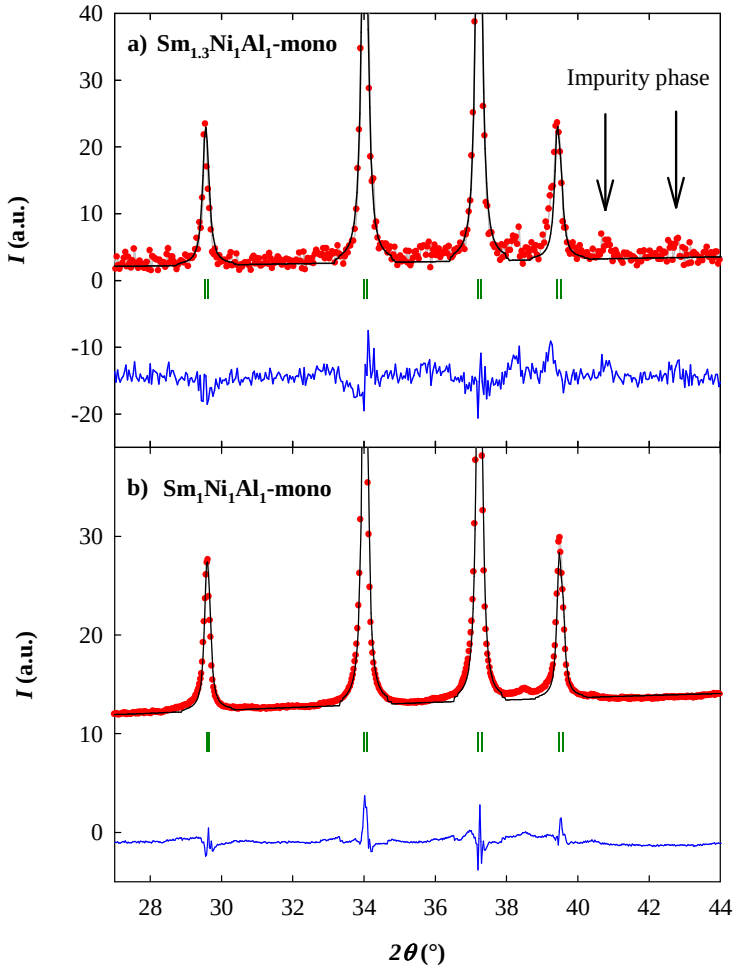

Figure 4.15: Comparison of diffraction pattern of SmPdAl monocrystalline compounds. Red points represent observed relative intensities, black line is their refinement. Impurity phases present in the $Sm_{1.3}Ni_1Al_1$ (marked by arrows) are not present in the $Sm_1Ni_1Al_1$ sample.

The already prepared SmNiAl polycrystalline sample consists of two ZrNiAl-type phases, monocrystalline sample on the other hand is single-phased.

This difference is explained through the different preparation methods and their influence on the quality of the samples.

Polycrystalline sample consists of many grains. Therefore the possible local shift of composition and especially lattice imperfections of each grain cause distribution of the lattice constants *a* and *c* over a specific non-zero range. Since the lattice of SmNiAl is at the border of the critical values of *c/a*, the existence of the non-zero interval of the lattice parameters around the values of forbidden c/a gap leads to the fact that some of the grains may be in the "high *c/a*" phase while others are to be found in the "low *c/a*" phase.

In the case of monocrystalline sample, only one of the grains gets the priority to form the neck in the Czochralski method. Afterwards it is only this grain that propagates into the phase of the resulting ingot. The whole sample is then made by either "high *c/a*" or "low *c/a*" phase.

Later, pieces with orientation in two main directions of the crystal structure were prepared.

4.2.2 SmPdAl structural results

As stated in previous results (see Chapter 1), SmPdAl is expected to undergo structural phase transition in temperatures above room temperature. Various micro- and macroscopic measurements were performed to investigate this temperature region. From the microscopic view, it was studied by means of X-ray powder diffraction. It was performed on both mono- and polycrystalline samples in the temperature range from RT up to 750 K where the sample undergoes an irreversible phase transition to a different phase. We didn't perform detailed research on this phase since it is not object of our study. Structural parameters were obtained using program Fullprof. Resulting lattice parameters *a*, *c* and temperature dependence of their ratio *c/a* and of volume of the formula unit $V_{f.u.}$ are shown in Tables 6, 7 and Figures 4.19, 4.20.

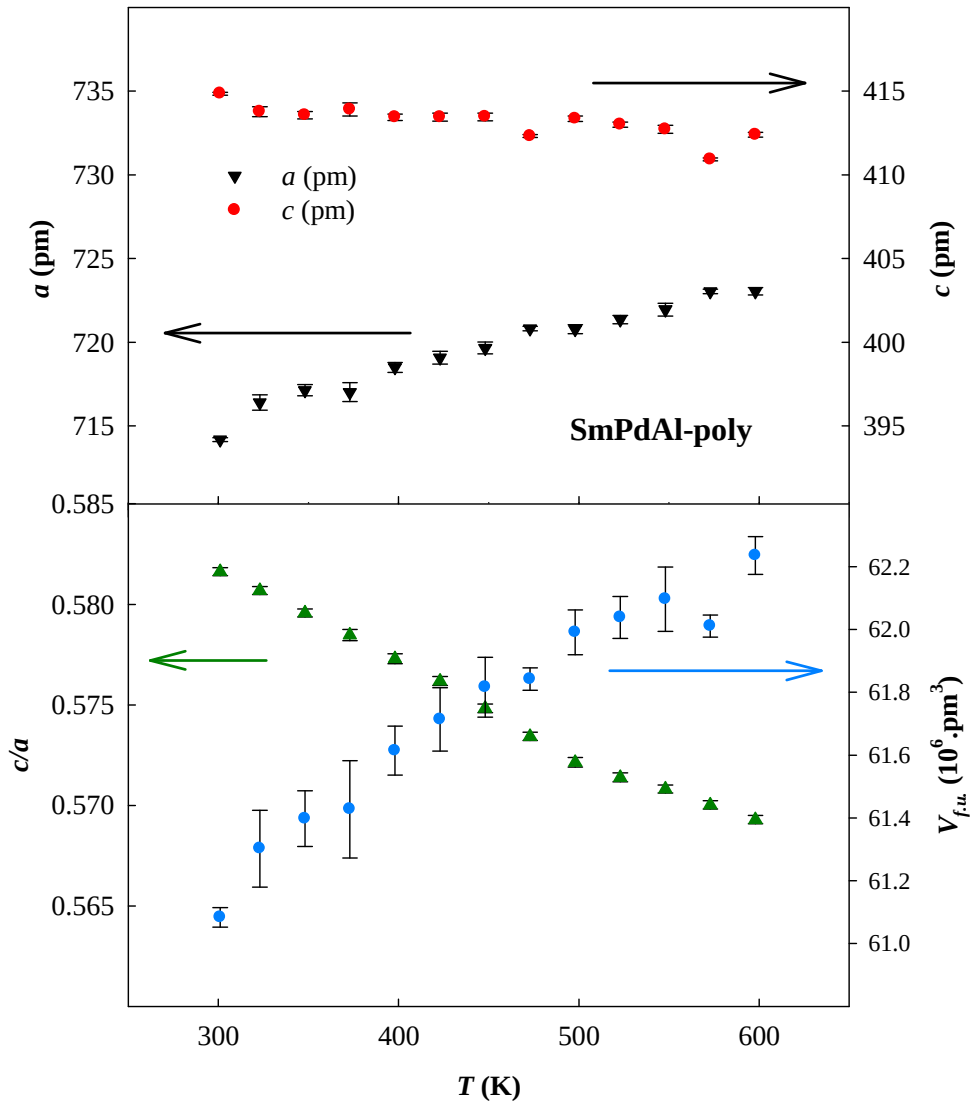

Figure 4.19: Evolution of the structure parameters of SmPdAl-polycrystalline sample in dependence on the temperature.

Table 6: Temperature evolution of the structure parameters of SmPdAl-poly. Agreement factor R_{Bragg} of the given fitting procedure is displayed too.

T (K)	a (pm)		c (pm)		c/a		$V_{f.u.}$ (10^6.pm^3)		R_{Bragg}
301	714.19	(0.12)	414.84	(0.08)	0.58085	(20)	61.08	(0.03)	13.1
323	716.41	(0.46)	413.76	(0.30)	0.57754	(20)	61.30	(0.12)	17.5
348	717.14	(0.33)	413.56	(0.21)	0.57668	(20)	61.40	(0.09)	16.0
373	717.02	(0.56)	413.90	(0.39)	0.57725	(28)	61.43	(0.15)	36.4
398	718.50	(0.29)	413.44	(0.19)	0.57542	(24)	61.61	(0.08)	14.0
423	719.08	(0.38)	413.44	(0.24)	0.57496	(23)	61.71	(0.10)	16.8
448	719.66	(0.36)	413.46	(0.23)	0.57452	(22)	61.82	(0.10)	15.8
473	720.82	(0.14)	412.31	(0.09)	0.57201	(22)	61.84	(0.04)	10.6
498	720.78	(0.27)	413.35	(0.17)	0.57348	(23)	61.99	(0.07)	14.5
523	721.36	(0.25)	413.00	(0.16)	0.57253	(22)	62.04	(0.07)	15.5
548	721.95	(0.39)	412.71	(0.24)	0.57166	(21)	62.10	(0.10)	18.8
573	723.03	(0.13)	410.92	(0.08)	0.56833	(21)	62.01	(0.04)	10.6
598	723.04	(0.23)	412.39	(0.14)	0.57035	(21)	62.24	(0.06)	14.3

Table 7: Temperature evolution of the structure parameters of SmPdAl-monocrystalline sample. Agreement factor R_{Bragg} is displayed too.

T (K)	a (pm)		c (pm)		c/a		$V_{f.u.}$ (10^6.pm^3)		R_{Bragg}
299	713.96	(0.12)	415.26	(0.08)	0.58163	(20)	61.105	(31)	9.2
323	714.75	(0.11)	415.04	(0.08)	0.58068	(20)	61.208	(31)	9.0
348	715.62	(0.11)	414.75	(0.08)	0.57957	(20)	61.314	(31)	9.0
373	716.45	(0.16)	414.45	(0.11)	0.57847	(28)	61.412	(43)	8.9
398	717.22	(0.13)	414.05	(0.10)	0.57729	(24)	61.485	(38)	9.6
423	718.10	(0.13)	413.76	(0.09)	0.57619	(23)	61.593	(36)	9.7
448	718.90	(0.13)	413.24	(0.08)	0.57482	(22)	61.653	(34)	11.3
473	719.77	(0.12)	412.74	(0.08)	0.57343	(22)	61.728	(34)	11.3
498	720.56	(0.14)	412.26	(0.09)	0.57214	(23)	61.790	(37)	11.8
523	720.94	(0.13)	411.94	(0.09)	0.57139	(22)	61.807	(35)	12.0
548	721.37	(0.12)	411.77	(0.08)	0.57082	(21)	61.855	(32)	11.0
573	722.00	(0.12)	411.56	(0.08)	0.57002	(21)	61.932	(33)	11.4
598	722.64	(0.12)	411.39	(0.08)	0.56929	(21)	62.016	(33)	12.9
623	723.09	(0.38)	411.50	(0.26)	0.56908	(66)	62.11	(0.10)	23.3
648	723.57	(0.31)	411.02	(0.21)	0.56804	(53)	62.12	(0.08)	30.7
673	724.04	(0.36)	410.81	(0.24)	0.56739	(61)	62.17	(0.10)	35.8
698	724.67	(0.42)	410.58	(0.29)	0.56658	(73)	62.24	(0.12)	36.5
723	725.48	(0.46)	410.15	(0.31)	0.56534	(79)	62.32	(0.13)	41.6
748	726.39	(1.03)	409.66	(0.67)	0.5639	(17)	62.40	(0.28)	58.2

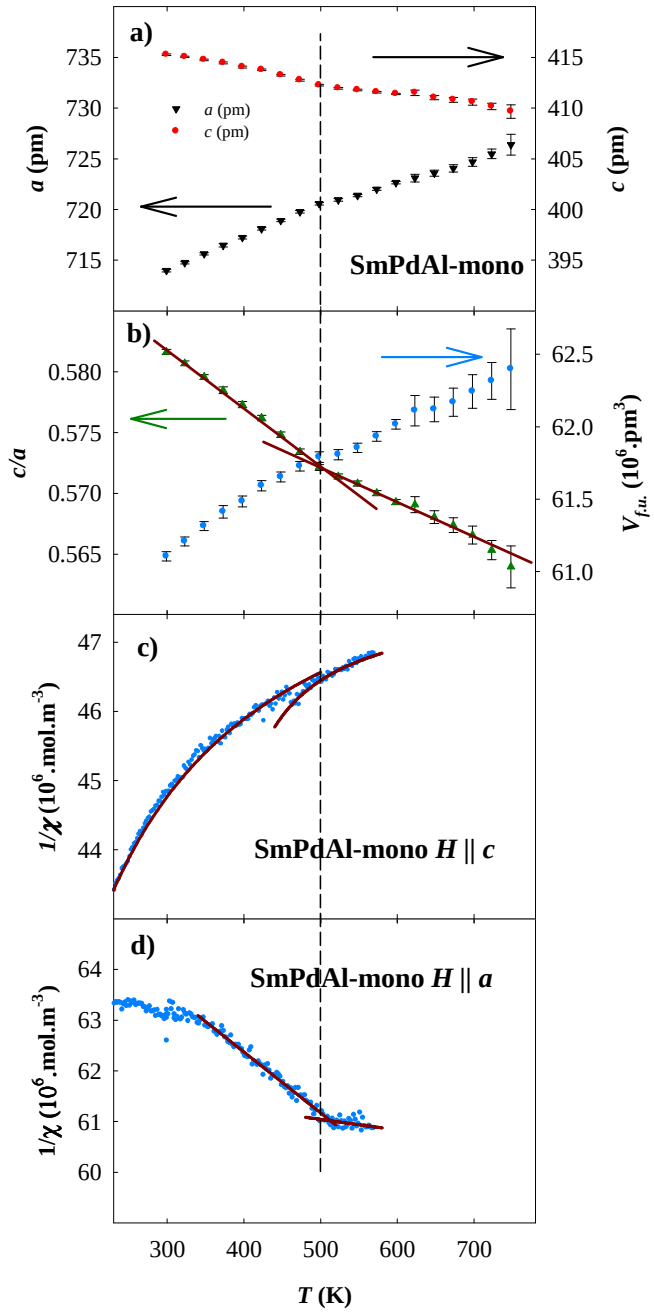

Figure 4.20: Temperature evolution of the structure parameters of the monocrystalline SmPdAl sample (parts a) and b) of the figure). Parts c) and d) display temperature dependencies of inverse susceptibility $1/\chi$, with the external magnetic field applied along- and perpendicular to the *c*-axis, respectively. Modified Curie-Weiss law was applied to the data in the orientation of field along *c*-axis. The lines in d) are used to guide the reader's eye. The vertical line displays phase transition of a higher order as determined from the XRD data.

Since the monocrystalline sample is of a higher quality (see Chapter 4.2.1.2) we will take its results as primary and the results of the polycrystalline one will be taken into account as a supporting data.

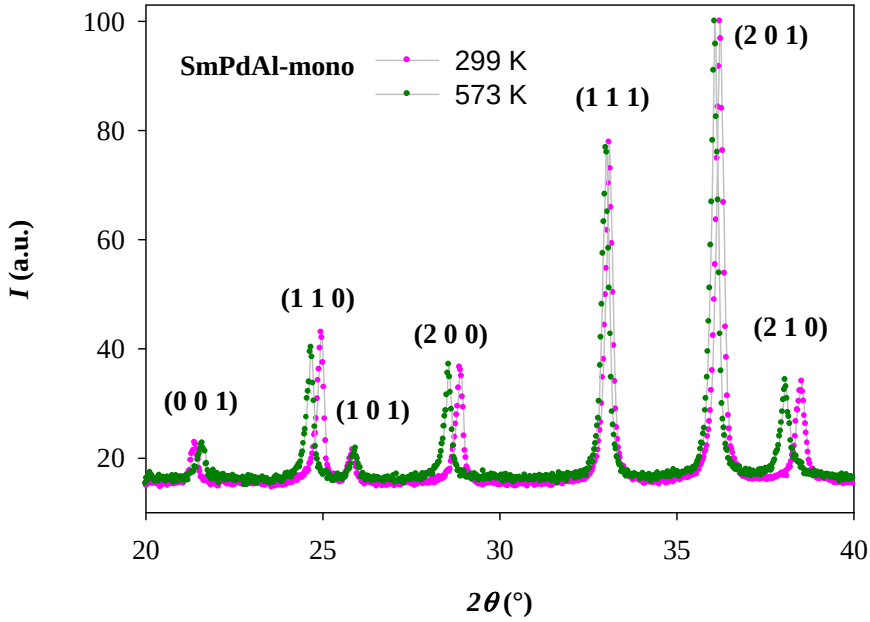

Figure 4.21: Comparison of diffraction patters of the SmPdAl monocrystalline sample at room temperature and at 573 K.

It can be clearly seen from the comparison of the diffraction patterns in Figure 4.21 and from Figures 4.19 and 4.20 a), b) that SmPdAl is single phased in the whole temperature range. The first order phase transformation is not present in the studied temperature range. It can be nevertheless seen, that different types of reflections shift in different ways – e.g. The (001) peaks shift to higher angles, whereas the (200) reflection moves to lower angle with increasing temperature. Similar property could be observed for compunds that exhibit the step-like change of the lattice with skipping of the forbidden values of the c/a (e.g. TbNiAl [07]). Change in the derivative of *c/a* ratio vs. temperature dependence is observed at around 500 K. The change may be connected with higher order phase transition.

The presence of higher-order phase transformation is supported by anomalies visible on the data of magnetic susceptibility. The dependence of $1/\chi$ vs. temperature of the monocrystalline SmPdAl is shown in the Figure 4.20 c) and d). In the case of the field oriented along the *c*-axis at 460 K there is a step-like change of the $1/\chi$ dependency, dividing the paramagnetic region into two parts with different characters. Magnetic properties

themselves are discussed in the following part. In the case of the field oriented perpendicular to the *c*-axis there is visible a clear change of the slope of the measured curve at 510 K. Both of the temperatures are in agreement with change of the derivative of the lattice parameters at 500 K as obtained from X-Ray diffraction measurement.

Existence of higher-order phase transformation instead of the first order phase transformation is in accordance with previously studied systems. [15]. This result supports the idea that the first-order phase transition connected with coexistence of two phases tends to happen at lower temperatures (see Figure 4.22). Due to higher temperature the atoms have higher kinetic energy, thus their thermal movement is larger. This enables the compound to cross the forbidden *c/a* value states, which are not preferred at lower temperatures. However, there is a criticality still present as can be seen from the above mentioned results. This critical behaviour takes place at values of *c/a* around 0.571, which is in the middle of the forbidden gap values (0.565 – 0.575). This brings us to the idea that at higher temperatures the gap becomes narrower but does not disappear totally and its influence can still be observed.

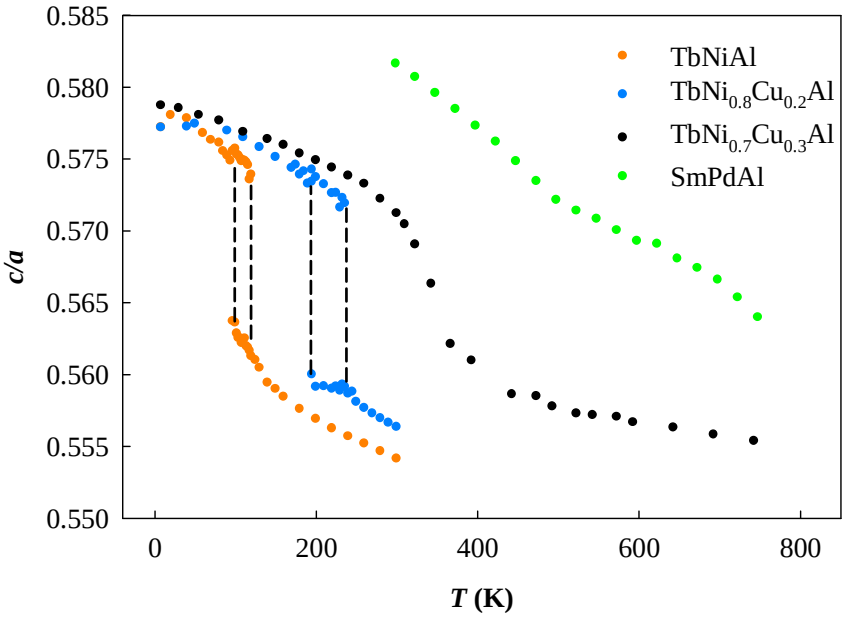

Figure 4.22: Temperature evolution of *c/a* ratio of various compounds (data for $TbNi_{1-x}Cu_xAl$, x= 0, 0.2, 0.3 taken from [15]. Coexistence of both *c/a* phases is present when the area of forbidden values is reached at lower temperatures.

4.2.3 SmPdAl magnetic results

Measurement of the temperature dependence of magnetisation of the SmPdAl-monocrystalline sample with magnetic field applied along and perpendicular to the *c*-axis is shown in Figure 4.23.

Interesting behaviour was observed in the paramagnetic region, if the field is applied perpendicular to the *c*-axis as can be seen from Figure 4.23 b). At temperature T_j = 260 ± 10 K magnetisation of the sample exhibits its local minimum. Above this point the magnetisation starts to rise with increasing temperature. This is not a typical behaviour for rare earth-based compounds. Their magnetic behaviour in the ground state is described by applying Hund's rules. We obtain the value of total angular momentum *J* (see chapter 2.4) using which it is possible to calculate effective magnetic moment μ_{eff}. The excited state of Sm is quite close to the ground state, in comparison to the other rare-earth elements. Thus for Sm the excited states have to be taken into account. The first excited multiplet J = 7/2 is at a distance of only 1400K above the ground state with J = 5/2. As stated in Ref. [16],

the admixture of the J = 7/2 and higher states into the J = 5/2 ground state are of the order of ~200 K/1400 K or 10 to 20%. The admixtures are too small to be responsible only by themselves for such a significant influence on the magnetic behaviour. Their effects are however enlarged by mixing of the admixtures together. Consequence of this is the increase of the effective magnetic moment of Sm ion with temperature as can be seen from (Figure 4.24). This is qualitatively same behaviour as observed in our case. The only difference is the critical temperature *Tj* where the minimum occurs, it is shifted by the influence of the crystal surrounding of the Sm^{3+} ion in our compounds.

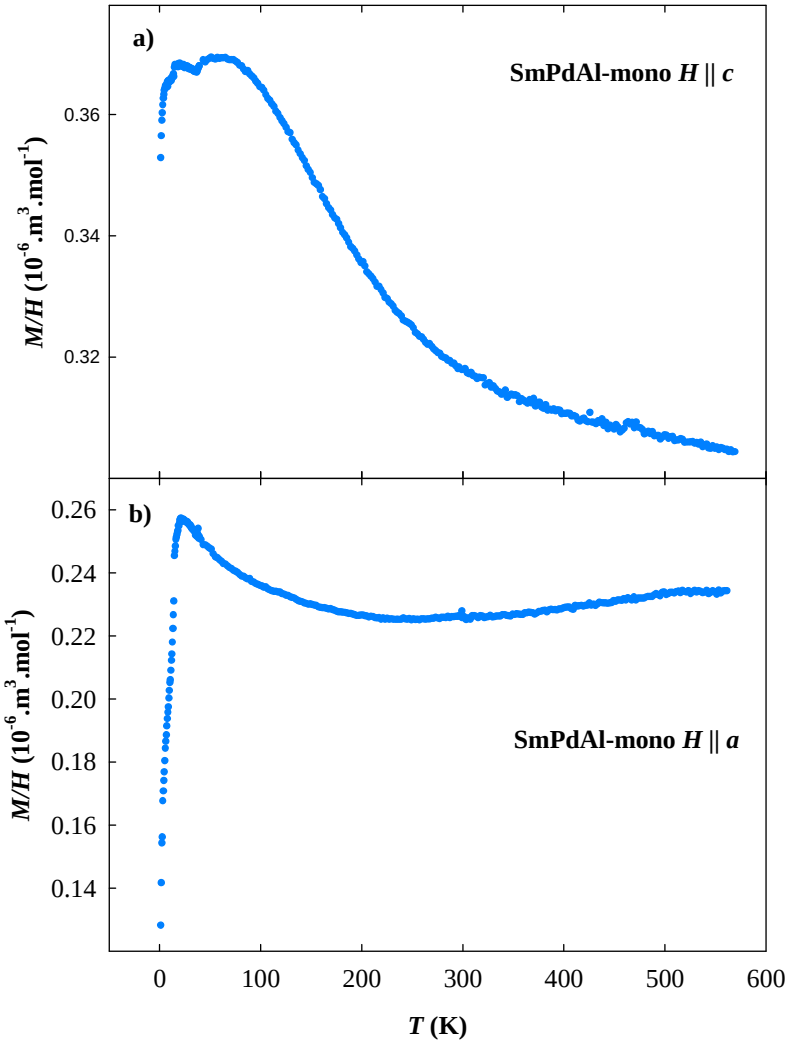

Figure 4.23: Magnetic measurement of the SmPdAl-mono with applied magnetic field $\mu_0 H$ = 0.5T. The bump in part b) at 300 K is caused by connecting data from the high- and low-temperature experiments.

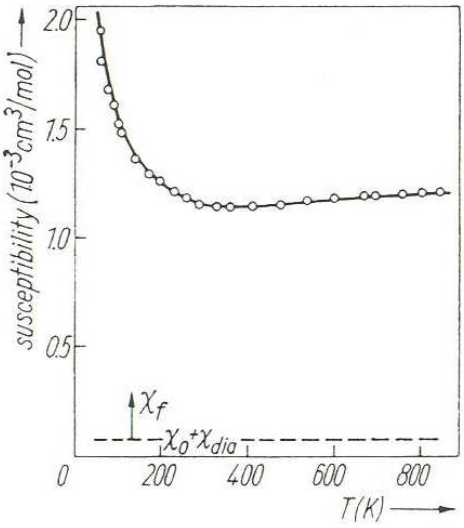

Figure 4.24: Behaviour of the magnetic susceptibility of the Sm^{3+} ion versus temperature. Picture taken from [16].

In the paramagnetic region modified Curie-Weiss law (equation 8) was applied to the $1/\chi$ dependency on temperature (as shown in Figure 4.20 c). Obtained parameters are listed in the following Table 8.

Table 8: Parameters obtained from applying Curie-Weiss law

Orientation of the field *H*	Temperature region (K)	μ_{eff} (μ_B)	χ_0 ($10^8.m^3/mol$)	θ_p (K)
H ∥ *c*	155 – 460	0.60 (0.03)	2.02 (0.08)	23 (10)
	462 – 570	0.240 (42)	2.0976 (92)	335 (29)
H ⊥ *c*	35 - 225	0.4003 (49)	1.4898 (20)	-53.0 (1.7)

The obtained values of the effective magnetic moment μ_{eff} are smaller than the one of Sm^{3+} ion, which equals 0.85 μ_B. The lowering may be caused by the influence of the crystal field as reported for other rare earths [17-22]. The reason for such significant uncertainties in the case of *H* applied along the *c*-axis in the temperature range 155 – 460 K is that the parameters resulting from applying Curie-Weiss law were strongly correlated with the choice of starting temperature of the temperature region.

Other characteristic obtained by applying Currie-Weiss law is θ_p that may tell us more about the character of the magnetic exchange interactions. Negative values mean that antiferromagnetic interactions are dominant, positive on the other hand represent majority of ferromagnetic interactions. For the field *H* applied perpendicular to the *c*-axis the values of θ_p are negative (Table 8), which suggests that antiferromagnetic interactions are the main ones within the basal plane. While applying the field *H* along *c*-axis value close to zero was obtained (Table 8).

SmPdAl becomes magnetically ordered at low temperatures below ordering temperature - as determined from the specific-heat data - T_c = 15.3 ± 0.2 K. This temperature is marked by a black vertical line in the Figure 4.25. Anomalies corresponding to the estimated ordering temperature visible by the other used methods (magnetisation and resistivity measurements) are in good agreement with this temperature, as can be seen from the Figure 4.25.

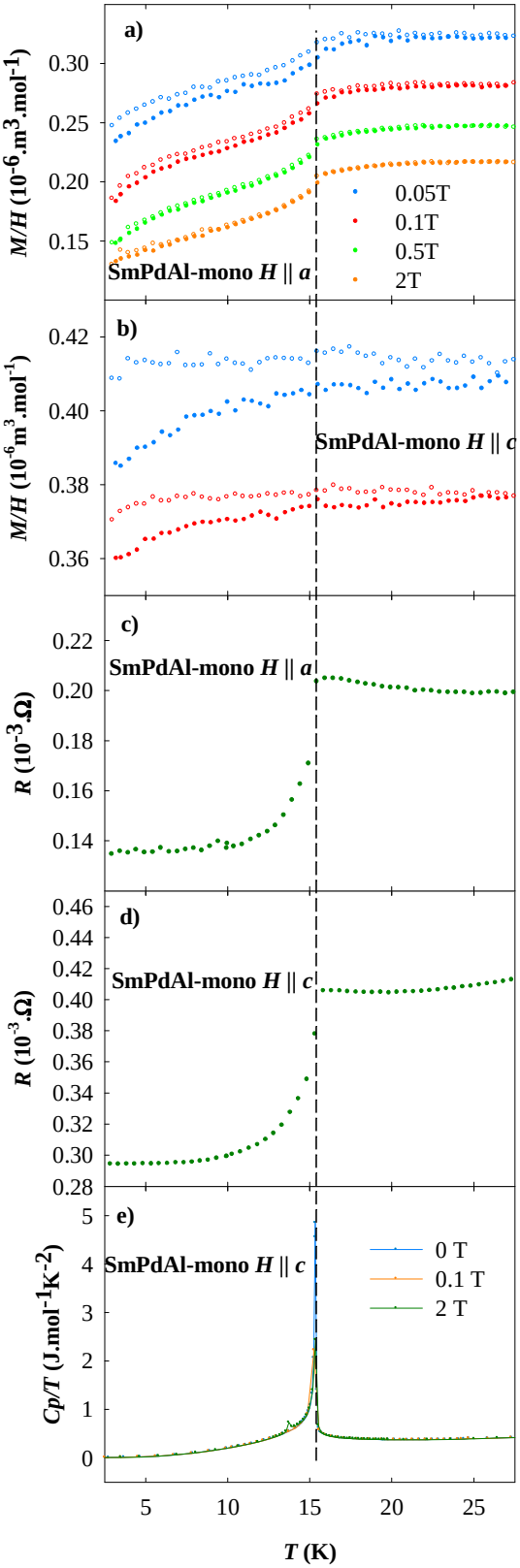

Figure 4.25: Temperature dependence of magnetisation, resistance and specific heat of SmPdAl in the vicinity of the magnetic ordering temperature. The vertical line displays the phase transition as determined from the specific-heat data.

Character of the magnetic interactions is reflected in the magnetisation curves. Behaviour of SmPdAl while applying field perpendicular to the *c*-axis (Figure 4.27 b)) is typical for first part of antiferromagnetic magnetisation curve (see Figure 4.26). In the DyNiAl sample critical value of magnetic field to induce magnetic transition is between 1 – 2 T. In our case the magnetic field needed to induce such a transition is much higher than maximum *H* used, which was 14 T.

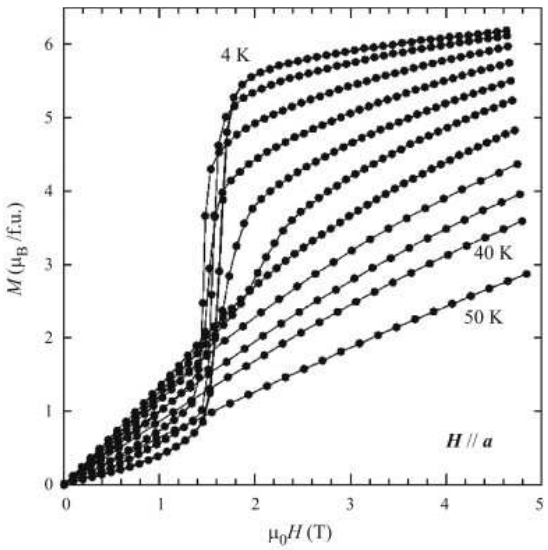

Figure 4.26: Magnetisation curve of DyNiAl as a representation of compound with antiferromagnetic behaviour. Picture taken from [23].

Antiferromagnetic character of magnetisation curve corresponds to the negative values obtained from applying Curie-Weiss law. In the case of field applied along the *c*-axis the sample at low temperatures does show neither ferromagnetic nor antiferromagnetic behaviour.

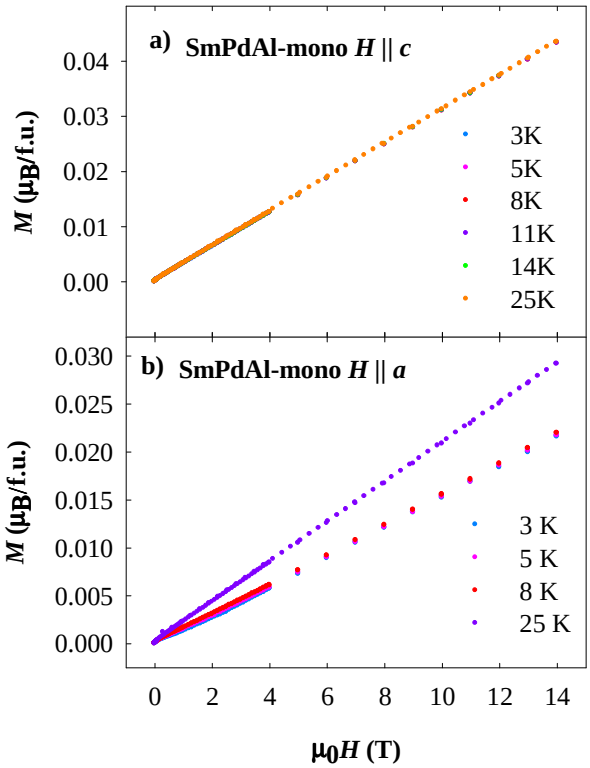

Figure 4.27: The magnetisation curves of the SmPdAl monocrystalline compound.

4.2.4 SmNiAl Structural results

As in the case of SmPdAl, SmNiAl is expected to undergo a structural transformation at temperatures above room temperature (see chapter 1). This region was investigated by the same methods as SmPdAl compound.

High-temperature X-ray powder diffraction was performed on both polycrystalline and monocrystalline samples. Obtained lattice parameters *a*, *c*, their ratio *a/c* and volume of the formula unit $V_{f.u.,}$ together with R-Bragg factor are listed in the following Tables 9 and 10 plotted in Figures 4.28 and 4.29.

Table 9: Results of HT X-ray powder diffraction of the SmNiAl polycrystalline sample. Agreement factor R_{Bragg} of the given fitting procedure is displayed too.

	T (K)	a (pm)		c (pm)		c/a		$V_{f.u.}$ (10^6.pm^3)		R_{Bragg}
phase 1	303	696.81	(0.06)	402.81	(0.04)	0.57808	(11)	56.461	(16)	6.41
	373	698.31	(0.05)	402.34	(0.03)	0.57616	(09)	56.636	(13)	5.38
	473	701.47	(0.07)	400.95	(0.05)	0.57159	(13)	56.953	(19)	7.32
	573	704.71	(0.07)	399.17	(0.05)	0.56643	(12)	57.224	(18)	6.42
	673	708.52	(0.15)	397.40	(0.11)	0.56088	(27)	57.589	(40)	13.5
phase 2	303	710.48	(0.20)	396.64	(0.19)	0.55827	(42)	57.797	(60)	23.4
	373	711.62	(0.15)	396.35	(0.15)	0.55696	(32)	57.940	(46)	16.7
	473	713.37	(0.22)	396.03	(0.21)	0.55515	(47)	58.178	(68)	16.3
	573	714.54	(0.19)	395.72	(0.18)	0.55381	(40)	58.323	(58)	11.6
	673	715.02	(0.26)	395.58	(0.21)	0.55325	(50)	58.383	(74)	18.3

Table 10: Results of HT X-ray powder diffraction of the SmNiAl mono-crystalline sample. Agreement factor R_{Bragg} of the given fitting procedure is displayed too.

T (K)	a (pm)		c (pm)		c/a		$V_{f.u.}$ (10^6.pm^3)		R_{Bragg}
302	696.80	(0.09)	402.75	(0.07)	0.57800	(17)	56.449	(24)	9.42
323	697.55	(0.07)	402.54	(0.05)	0.57707	(14)	56.541	(19)	10.3
348	698.48	(0.08)	402.23	(0.06)	0.57586	(15)	56.648	(21)	9.68
373	699.41	(0.07)	401.86	(0.05)	0.57457	(13)	56.747	(19)	9.66
398	700.35	(0.08)	401.43	(0.06)	0.57318	(15)	56.839	(22)	10.5
423	701.34	(0.09)	400.98	(0.06)	0.57173	(16)	56.936	(24)	10.6
448	702.20	(0.08)	400.49	(0.06)	0.57034	(16)	57.006	(22)	11.5
473	703.02	(0.10)	400.04	(0.07)	0.56903	(18)	57.076	(27)	11.6
498	703.74	(0.10)	399.61	(0.07)	0.56784	(18)	57.130	(27)	11.2
523	703.80	(0.11)	399.61	(0.08)	0.56779	(20)	57.142	(29)	12.5
548	704.65	(0.11)	399.10	(0.08)	0.56638	(20)	57.206	(30)	10.7
573	705.71	(0.13)	398.49	(0.09)	0.56466	(23)	57.290	(34)	10.9

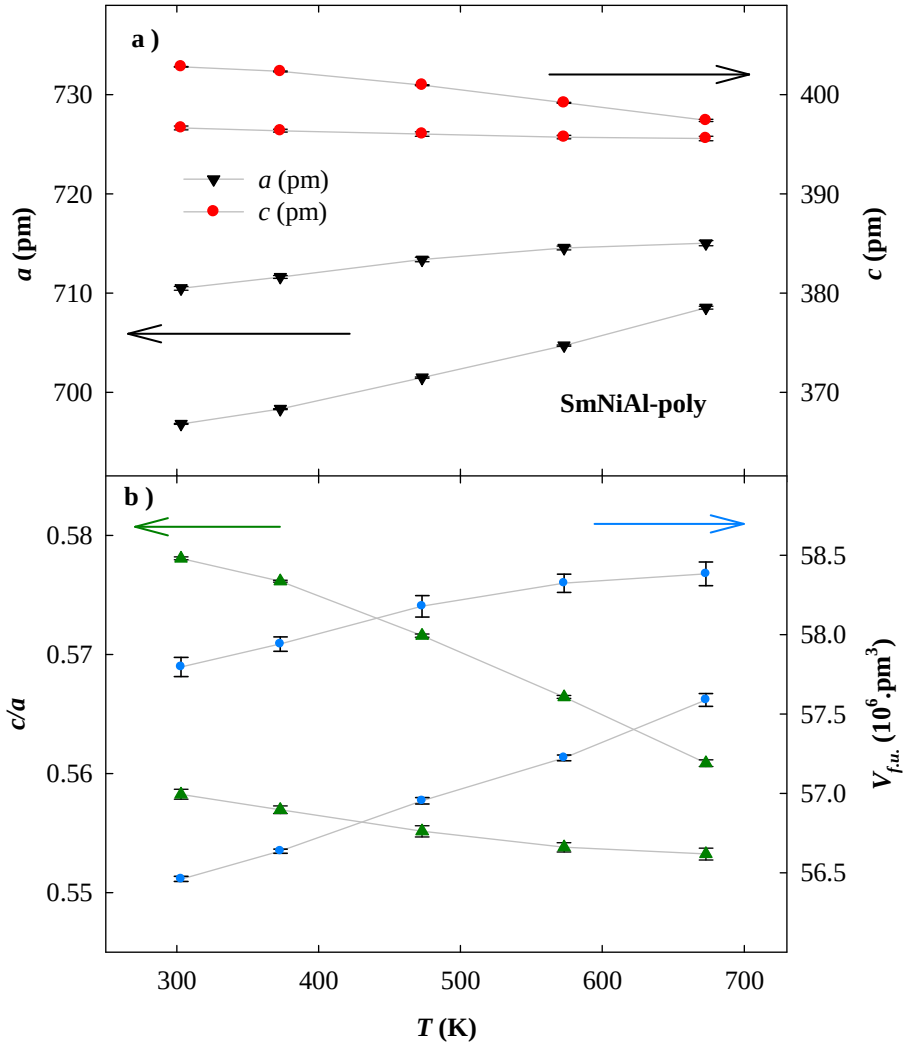

Figure 4.28: Temperature evolution of the lattice parameters *a*, *c*, their ratio *c/a* and $V_{f.u.}$ of the SmNiAl-polycrystalline sample. Lines are used as to guide the reader's eye.

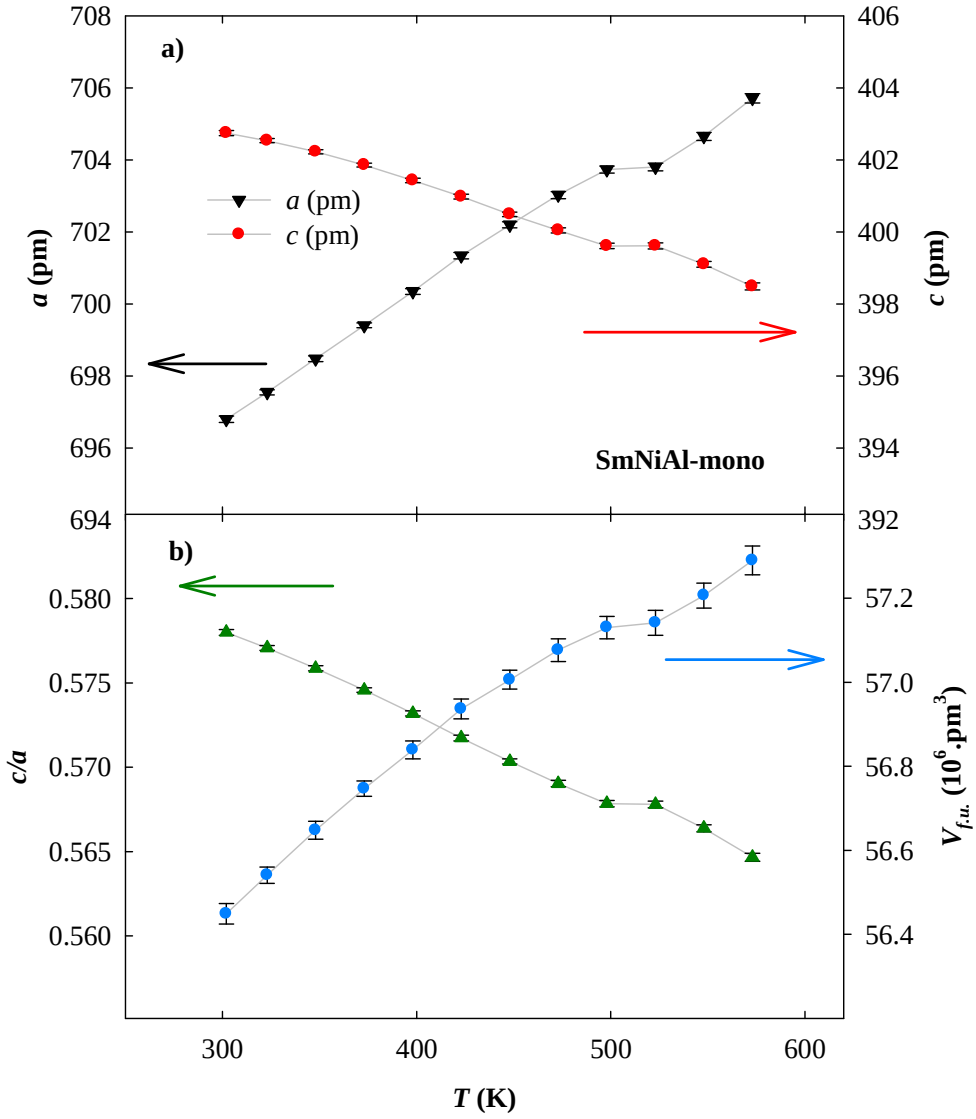

Figure 4.29: Temperature evolution of the lattice parameters *a*, *c* and their ratio *c/a* of the SmNiAl-monocrystalline sample. Lines are used as to guide the reader's eye.

In the polycrystalline SmNiAl both of the phases - characterised by the low *c/a* and high *c/a* ratio - are present in the whole temperature range. Their coexistence is enabled thanks to relative wide interval of lattice parameters distribution. Ratio of *c/a* of the "high *c/a*" phase, which is more populated – as determined from intensity of the peaks - changes from *c/a* = 0.5781 ± 0.0001 at room temperature to *c/a* = 0.5664 ± 0.0001 at 573 K. The *c/a* ratio of the "low *c/a*" phase, which is less populated, changes significantly less: *c/a* = 0.5583 ± 0.0004 at room temperature, *c/a* = 0.5538 ± 0.0004 at 673 K.

On the other hand monocrystalline sample stays single-phased for all the temperatures measured. Here the *c/a* ratio starts its temperature evolution at *c/a* = 0.5780 ± 0.0002 at room temperature and finishes at 0.5647 ± 0.0002 at 573 K. This is exactly the same behaviour as of the "high *c/a*" phase of the poly-crystalline sample. Again, as in the case of SmNiAl, the evolution of c/a exhibits criticality at temperature around 500 K.

4.2.5 SmNiAl Magnetic results

Measurement of temperature dependence of magnetisation of the SmNiAl-monocrystal with applied magnetic field parallel and perpendicular to the *c*-axis is shown in Figure 4.30.

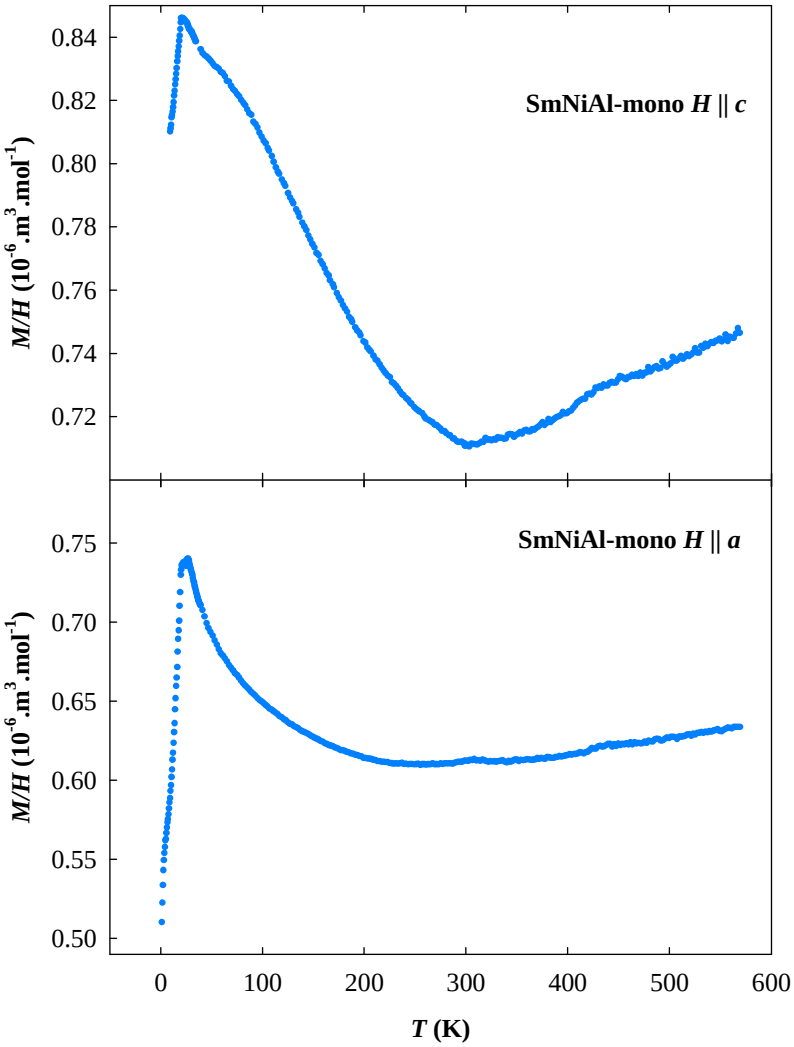

Figure 4.30: Dependency of the magnetisation vs. temperature of the SmNiAl-monocrystalline sample.

Again, as in case of SmPdAl, in the paramagnetic region at 256 K ± 10 K excited energy levels of Sm start to be occupied, resulting into increasing magnetisation of the compound with increasing temperature. In both cases - $H \parallel c$ and $H \perp c$- there is a certain anomaly visible at T = 300 K, this may be caused by connecting data from LT and HT experiment.

Modified Curie-Weiss law was applied to the $1/\chi$ dependency on temperature in the paramagnetic region. Parameters obtained are listed in Table 11.

Table 11: Parameters obtained from applying Curie-Weiss law.

Orientation of the field H	Temperature region (K)	μ_{eff} (μ_B)	χ_0 (10^8.m^3/mol)	θ_p (K)
$H \parallel c$	130 - 304	1.126 (26)	4.400 (18)	-43.4 (5.5)
$H \perp c$	30 - 228	0.7063 (45)	3.9836 (37)	-38.104 (0.72)

If the field is applied perpendicular to the c-axis the value of μ_{eff} = 0.7063 ± 0.0045 is close to the values of Sm^{3+} ion, which equals 0.85 μ_B. Negative values of θ_p mean dominating antiferromagnetic character of magnetic interactions.

At low temperatures below 20.3 ± 0.3 K; as determined from specific heat-capacity measurement; the SmNiAl compound becomes magnetically ordered. The same ordering temperature was confirmed by means of the other measurement methods as magnetic or electrical resistivity measurements (see Figure 4.31).

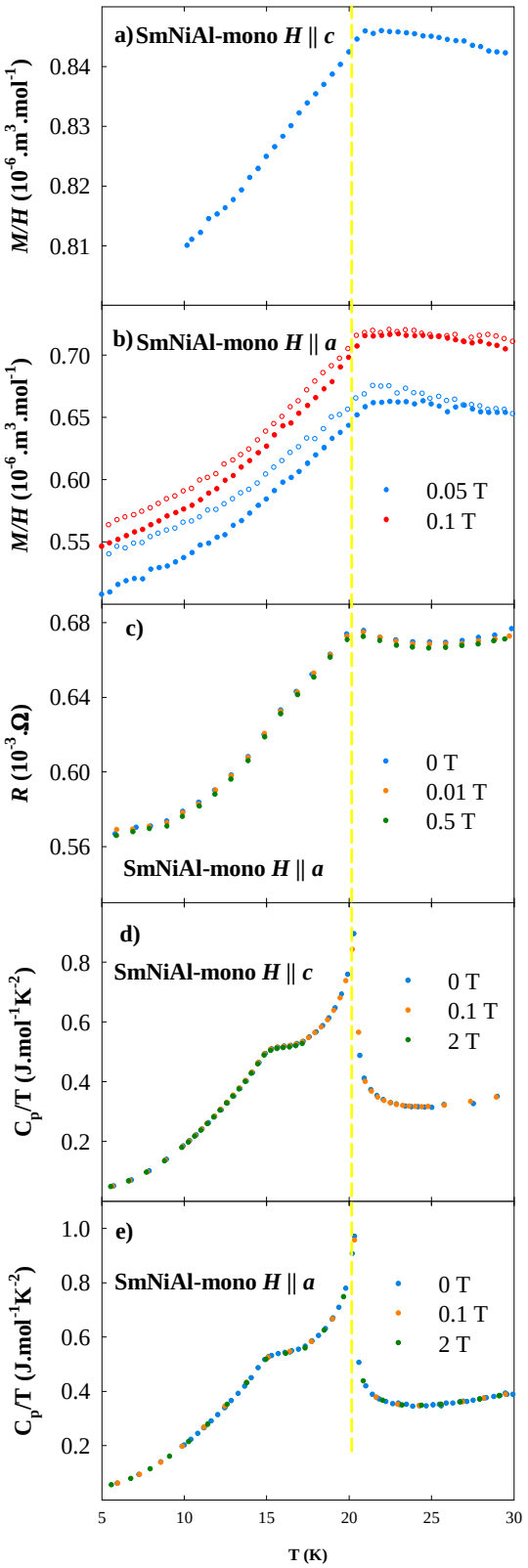

Figure 4.31: Temperature dependence of magnetisation, resistance and specific heat of SmPdAl in the vicinity of the magnetic ordering temperature. The vertical line displays the phase transition as determined from the specific-heat data.

Character of magnetic interactions is reflected in the magnetisation curves measurements (see Figure 4.32). As in case of SmNiAl the sample exhibits behaviour typical for antiferromagnetic compounds. Field-induced magnetic transition happens at temperatures much higher than 14 T.

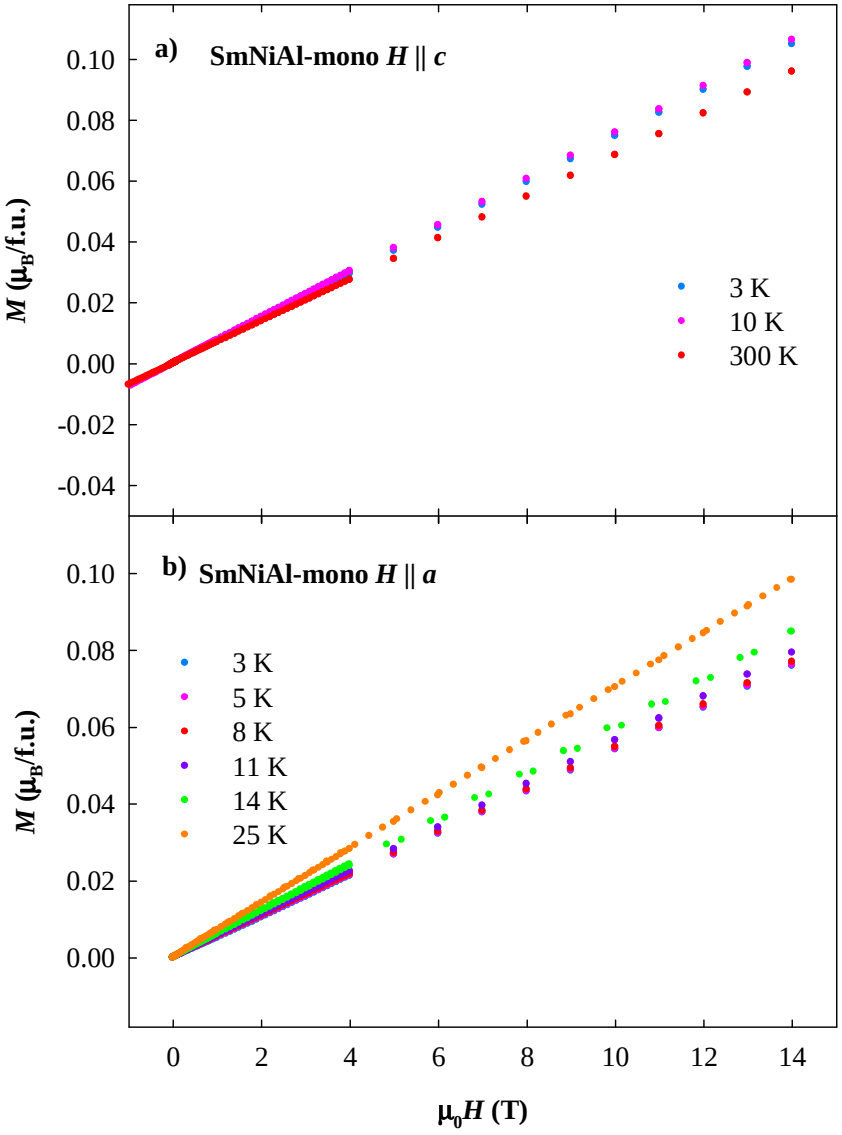

Figure 4.32: The magnetisation curves of SmNiAl monocrystalline sample.

5 Conclusions

The $Ce_{1-x}Y_xPdAl$ samples with composition x = 0.2, 0.3, 0.8 exhibit single phase, whereas the compounds with x = 0.4, 0.5 exhibit coexistence of two different phases over the whole studied range of temperatures (8-773 K). The coexistence of the phases is connected with a gap of forbidden values of *c/a* which evolves with temperature and composition. This is the main difference from previously studied systems, where the substitution on the position of transition-metal element causes changes in both of the layers, whereas in our case of (Ce,Y)PdAl compounds, the substitution occurs only in one of the hexagonal layers altering along the *c*-axis.

The SmPdAl sample - both in polycrystalline and monocrystalline form - is single phased in the whole temperature range (300 – 748 K). However a criticality in evolution of *c/a* is present at temperature ≈ 500 K. Anomalies visible on the data of magnetisation and electrical resistivity correspond to anomaly visible on the data of structural evolution. Explanation based on enhanced thermal movement of the atoms is proposed. In paramagnetic region compound exhibited local minima, this was caused by admixtures of excited energy states into the ground energy state of the Sm atoms. The magnetic ordering temperature was determined as T_c = 15.3 ± 0.2 K. Character of the magnetic interactions is mainly antiferromagnetic.

The polycrystalline SmNiAl exhibits coexistence of both phases in the whole temperature range (300 – 673 K), whereas monocrystalline sample stays single-phased in the range from 300 to 573 K. Coexistence in polycrystalline sample is enabled thanks to relative wide interval of lattice parameters distribution among the huge number of the grains. Again a criticality in evolution of *c/a* is present at temperature around 500 K. The same behaviour in the paramagnetic region as for SmPdAl was observed. Antiferromagnetic interactions are dominant in the sample. Ordering temperature T_c was determined as 20.3 ± 0.3 K.

6 References

[01] F.Merlo, S.Cirafici, F.Canepa, Journal of Alloys and Compounds 266 (1998) 22-25.

[02] J.Jarosz, E.Talik, T.Mydlarz, J.Kusz, H.Böhm, A.Winiarski, Journal of Magnetism and Magnetic Materials 208 (2000) 169-180.

[03] E.Talik, M.Skutecka, J.Kusz, H.Böhm, J.Jarosz, T.Mydlarz, A.Winiarski, Journal of Alloys and Compounds 325 (2001) 42-49.

[04] G.Ehlers, H.Maletta, Zeitschrift für Physik B 99 (1996) 145-150.

[05] A.Dönni, H.Kitazawa, P.Fischer, F.Fauth, Journal of Alloys and Compounds 289 (1999) 11-17.

[06] J. Prchal, H. Kitazawa, T. Furubayashi, : PHYSICA B-CONDENSED MATTER 378-80 (2006) 1102-1104

[07] J.Prchal, P.Javorský, H.Kitazawa, F.de Boer, M.Diviš, J.Rusz, A.Dönni, S.Daniš, V.Sechovský, Physical Review B 77 (2008) 134106; and references therein

[08] J.Prchal, P.Javorský, M. Dopita, O. Isnard, V.Sechovský, Journal of Alloys and Compounds 408-412 (2006) 155-157

[09] J.Prchal, H.Kitazawa, O.Suzuki, Journal of Alloys and Compounds 437 (2007) 117-119.

[10] A.Dönni, L. Keller, H.Kitazawa, J.Prchal, P.Fischer, Journal of Alloys and Compounds 464 (2008) 67-74

[11] http://www-ee.ccny.cuny.edu/www/web/crouse/EE339/Lectures/Bravais_Lattice.htm; as of 12th August 2010

[12] J.Rodriguez-Carvajal, Physica B 192 (1993) 55-69.

[13] H.M.Rietveld, Journal of Applied Crystallography 2 (1969) 65.

[14] http://www.xtal.iqfr.csic.es/Cristalografia/parte_06-en.html; as of 12th August 2010

[15] J. Prchal, F.R. de Boer, A.C. Moleman, P. Javorský, Acta Physica Polonica A 113 No.1 (2008) 335-338

[16] H. W. de Wijn, A. M. van Diefen, K. H. J. Buschov, Phys. Stat. Sol (b) 76 (1976) 11

[17] P.Javorský, Magnetism in RCuAl and RNiAl compounds; doctoral thesis, Prague, (1997)

[18] D.X.Li, T.Yamamura, S.Nimori, K.Koyama, Y.Shiokawa, Journal of Alloys and Compounds, 418 (2006) 151

[19] S.Baran, L.Gondek, J.Hernandez-Velasco, D.Koluorowski, A.Szytuła, Journal of Magnetism and Magnetic Materials, 300 (2006) 484

[20] E.Morosan, S.L.Bud'ko, P.C.Canfield, Physical Review B, 71 (2005)

[21] L.Gondek, S.Baran, A.Szytula, D.Kaczorowski, J.Hernandez-Velasco, Journal of Magnetism and Magnetic Materials, 285 (2005) 272

[22] W.Bazela, L.Gondek, B.Penc, A.Szytula, N.Stusser, A.Zygmunt, Acta Physica Polonica B, 32 (2001) 3387.

[23] J. Kaštil, P. Javorský, A. Andreev, Journal of Magnetism and Magnetic Materials 321 (2009) 2318-2321